



Attribution of ground-level ozone to anthropogenic and natural sources of NO_x and reactive carbon in a global chemical transport model

Tim Butler^{1,2}, Aurelia Lupascu¹, and Aditya Nalam^{1,2}

¹Institute for Advanced Sustainability Studies, Potsdam, Germany

²Institut für Meteorologie, Freie Universität Berlin, Germany

Correspondence: Tim Butler (tim.butler@iass-potsdam.de)

Abstract. We perform a source attribution for tropospheric and ground-level ozone using a novel technique which accounts separately for the contributions of the two chemically distinct emitted precursors (reactive carbon and oxides of nitrogen) to the chemical production of ozone in the troposphere. By tagging anthropogenic emissions of these precursors according to the geographical region from which they are emitted, we determine source/receptor relationships for ground-level ozone.

5 Our methodology reproduces earlier results obtained through other techniques for ozone source attribution, and also delivers additional information about the modelled processes responsible for intercontinental transport of ozone, which is especially strong during the spring months. The current generation of chemical transport models used to support international negotiations aimed at reducing the intercontinental transport of ozone show especially strong inter-model differences in simulated springtime ozone. Current models also simulate a large range of different responses of surface ozone to methane, one of the

10 major precursors of ground-level ozone. Using our novel source attribution technique, we show that emissions of NO_x from international shipping over the high seas play a disproportionately strong role in our model system to the hemispheric-scale response of surface ozone to changes in methane, as well as to the springtime maximum in intercontinental transport of ozone and its precursors. We recommend a renewed focus on improvement of the representation of the chemistry of ship NO_x emissions in current-generation models. We demonstrate the utility of ozone source attribution as a powerful model diagnostic tool,

15 and recommend that similar source attribution techniques become a standard part of future model inter-comparison studies.

1 Introduction

Tropospheric ozone plays a central role in the chemistry and self-cleansing capacity of the troposphere (Monks et al., 2015), but at high concentrations close to the ground, it is harmful to human health (Fleming et al., 2018) and vegetation (Mills et al., 2018). As well as being transported into the troposphere through exchange with the stratosphere, ozone can be formed through

20 chemical reactions in the troposphere involving two chemically distinct precursors: oxides of nitrogen (collectively NO_x); and reactive carbon species (Crutzen, 1973). Increases in tropospheric ozone since preindustrial times have been attributed primarily to increases in anthropogenic emissions of NO_x and methane, the most abundant reactive carbon species in the atmosphere (Wang and Jacob, 1998; Stevenson et al., 2013).



Ozone is long-lived enough in the troposphere to circumnavigate the Northern Hemisphere along the prevailing westerly winds (Jacob et al., 1999). Emissions of NO_x or reactive carbon in any Northern Hemisphere source region can thus contribute to the baseline ozone mixing ratio in any other region of the Northern Hemisphere. Due to seasonal variation in the lifetime of ozone, this effect is strongest in spring and weakest in summer (Fiore et al., 2009). The ambient ozone mixing ratio at any location is a combination of ozone transported from the hemispheric background, and in-situ photochemical production. Recent analyses of long-term trends in baseline ozone in western regions of North America (Parrish et al., 2017) and Europe (Derwent et al., 2018) have shown increasing trends since reliable measurements began in the 1980s until approximately 2000-2010, and indicate that these trends may be beginning to reverse.

Chemical Transport Models (CTMs) are commonly used to interpret observations of ozone, and synthesise understanding of the fundamental processes controlling its origin and fate in the atmosphere in order to project future trends (eg. Young et al., 2018). The range in values of surface ozone mixing ratio over the Northern Hemisphere simulated by contemporary CTMs is extremely high, requiring the use of a large ensemble of models (eg. HTAP, 2010; Young et al., 2018). When compared with available measurements of ozone for the Northern Hemisphere (eg. Schultz et al., 2017), ensembles of global CTMs are generally able to simulate the spatial distribution and seasonal cycles of surface ozone, but are consistently biased high in the Northern Hemisphere, and have difficulty in simulating long-term trends (Young et al., 2018). Potential sources of uncertainty in CTMs include uncertainties in their chemical mechanisms (the representations of the relevant chemical reactions and their rates), their representation of atmospheric transport processes, as well as exchange processes between the atmosphere and the surface of the Earth, including emissions of the ozone precursors NO_x and reactive carbon.

The most important class of reactions for the formation of ozone in the troposphere is the reaction of NO (nitric oxide) with a peroxy radical, which is itself formed during the oxidation of reactive carbon (Atkinson, 2000). During this process, the NO is converted to NO_2 (nitrogen dioxide), which can be rapidly photolysed, ultimately forming ozone and recycling NO. The ozone production efficiency of NO_x (the combined concentration of NO and NO_2) can vary significantly depending on the location and timing of the NO_x emissions. In the polluted boundary layer, NO_x is rapidly removed from the atmosphere through the reaction of NO_2 with OH, forming HNO_3 , which is subsequently lost via dry or wet deposition. Under less polluted conditions, NO_2 photolysis competes more effectively with HNO_3 production, allowing each unit of NO_x to react with a higher number of peroxy radicals before eventually being scavenged by OH, thus leading to higher ozone production efficiency per unit of NO_x . When NO_x is lofted into the free troposphere, its ozone productivity increases substantially (Jacob et al., 1996). Emissions of NO_x in the tropics are thus especially effective at producing tropospheric ozone due to being transported aloft due to deep convection (Zhang et al., 2016). NO_x emissions from both aircraft and lightning are also highly efficient at producing tropospheric ozone (Beck et al., 1992). Combustion of fossil fuels is the largest source of NO_x in the atmosphere (Galloway et al., 2008).

Lawrence and Crutzen (1999) first pointed out that international shipping can have a disproportionately high influence on tropospheric ozone due to the disperse nature of NO_x emissions from this source. Hoor et al. (2009) quantified the contribution to tropospheric ozone of NO_x emissions from different modes of transport (land, sea, and air), finding that aircraft emissions were most efficient at producing ozone (per molecule of NO_x emitted), followed by ships and then land transport. For near-



surface ozone however, NO_x emissions from ships were shown to have a higher influence than NO_x emissions from aircraft. Ozone production from ship NO_x is however highly uncertain in current CTMs. Kasibhatla et al. (2000) and von Glasow et al. (2003) showed that global CTMs, due to their coarse resolution (usually in the hundreds of km) do not resolve the chemistry of ship exhaust plumes, which tends to remove NO_x from the atmosphere more quickly than simulated by the global CTMs, which effectively instantly dilute these emissions into very large volumes. Vinken et al. (2011) introduced a method for parameterising ship exhaust plume chemistry using lookup tables in their global CTM, but this method has not been widely adopted by the modelling community. Modelling of ship NO_x and its effects on the atmosphere remains a challenge for global CTMs.

The term “reactive carbon” encompasses a very wide range of atmospheric constituents (eg. Chameides et al., 1992; Goldstein and Galbally, 2007; Heald and Kroll, 2020). In contrast to NO_x , most of the reactive carbon emitted to the atmosphere is not of anthropogenic origin, but rather emitted from the biosphere. In this study we restrict our definition to molecules which yield peroxy radicals (either hydroperoxy radicals HO_2 or organic peroxy radicals RO_2) during their gas phase oxidation, and thus contribute to ozone formation by potentially converting NO to NO_2 . This definition thus includes carbon monoxide (CO) and the large family of molecules known as Volatile Organic Compounds (VOC). The simplest VOC is methane, which is often considered separately from Non-Methane Volatile Organic Compounds (NMVOC) due to its very long lifetime in the troposphere. The ozone production potential of reactive carbon depends on the rate at which it is oxidised in the atmosphere, usually through reaction with the OH radical (Carter, 1994), as well as the subsequent chemistry of its oxidation products (Butler et al., 2011; Derwent, 2020). Most reactive carbon species have relatively short lifetimes in the troposphere due to their reaction with OH radicals. Methane, due to its exceptionally low reactivity is well-mixed in the troposphere. In contrast to other forms of reactive carbon, emissions of methane can contribute to ozone formation at any location in the troposphere where photochemical conditions are favourable (Fiore et al., 2008). Despite its low reactivity in comparison to other types of reactive carbon, methane is highly abundant, and has been shown to make a large contribution to tropospheric ozone (Wang and Jacob, 1998; Fiore et al., 2008; Stevenson et al., 2013; Butler et al., 2018).

PAN (Peroxyacetyl Nitrate) is an important reservoir species for both peroxy radicals and for NO_x (Fischer et al., 2014). Peroxyacetyl radicals are formed during the oxidation of a wide range of different types of NMVOC from a wide range of different sources. PAN is formed through reaction of peroxyacetyl radicals with NO_2 , primarily in the polluted boundary layer where both are abundant (Atkinson, 2000). The lifetime of PAN is strongly temperature dependent. At colder temperatures higher in the troposphere, PAN can be transported over long distances, and act as a source of NO_2 and peroxyacetyl radicals in remote regions upon subsidence and thermal decomposition (Fischer et al., 2014). The chemical mechanisms and reaction rate constants involved in the formation and decomposition of PAN vary widely between CTMs (Emmerson and Evans, 2009; Knote et al., 2015), leading to large inter-model differences in simulated PAN (Emmons et al., 2015). Fiore et al. (2018) has suggested that measurements of PAN at northern midlatitude mountaintop sites in spring could provide a useful constraint on CTMs, although the number of observations available is limited.

With careful interpretation, the results of ensembles of CTMs can be used to diagnose long-range transboundary transport of ozone, and to develop intercontinental source-receptor relationships, relating the effects of precursor emissions from differ-



ent regions of the Northern Hemisphere to mixing ratios of ground-level ozone in other regions of the Northern Hemisphere.

95 An example is the activity of the Task Force on Hemispheric Transport of Air Pollution (HTAP, 2010), which reports to the Convention on Long-Range Transboundary Air Pollution (CLRTAP) and thus informs international policymaking for the mitigation of air pollution. The TF-HTAP studies used a “perturbation” approach, in which a control simulation was compared with sensitivity simulations in which emissions of particular ozone precursors were reduced by 20%. Combined 20% reductions of global average methane and remote anthropogenic emissions of NO_x , CO, and NMVOC were shown to have an approximately

100 equal effect on annual average ozone as 20% reduction of local precursor emissions, indicating the strong role of long-range transport in influencing surface ozone in the Northern Hemisphere. Results derived from the phase one of the TF-HTAP exercise (and the phase two exercise described by Galmarini et al., 2017) are discussed in more detail by Fiore et al. (2009); Reidmiller et al. (2009); Huang et al. (2017); Jonson et al. (2018).

An alternative approach to the perturbation technique for source attribution is “tagging” (eg. Wang et al., 1998; Dunker et al., 2002; Grewe et al., 2010; Emmons et al., 2012; Derwent et al., 2015; Grewe et al., 2017; Butler et al., 2018). When applied to

105 ozone source attribution in a CTM, this technique involves labelling (or “tagging”) modelled ozone with the identity of either the geographical region in which it is chemically produced, or with the identity of the emitted precursor(s) which ultimately led to its production. A common problem faced by all tagging approaches is that the production of one molecule of ozone in the troposphere requires two precursors: one molecule of NO ; and one peroxy radical (produced during reactive carbon oxidation).

110 Should the ozone molecule inherit its tag from the emitted NO_x , the emitted reactive carbon, or in some other way? Butler et al. (2018) provides a detailed review of the different approaches to answering this question, including the trade-offs made in each case. Butler et al. (2018) also describe a novel and unique tagging methodology which allows separate attribution of tropospheric ozone to both its NO_x and its reactive carbon precursor, at the cost of extra computational expense compared with other tagging methodologies.

115 Tagging and perturbation approaches are complementary to each other (Clappier et al., 2017; Thunis et al., 2019). While tagging delivers information about the contribution of different emission sources to a pollutant of interest, perturbation studies deliver information about the sensitivity of pollutants to changes in emissions. In the absence of nonlinear chemical interactions, these two different approaches ultimately yield the same results, but for tropospheric ozone, which can under some circumstances show highly nonlinear interactions between its NO_x and reactive carbon precursors, these approaches can some-

120 times yield very different results (Grewe et al., 2010; Mertens et al., 2018). Since air pollution mitigation strategies must involve some change in emissions, perturbation studies will always be necessary for policy-relevant modelling of atmospheric chemistry. However, tagging studies on their own can play a role in helping to identify which emissions to mitigate (Grewe et al., 2010). When combined with perturbation studies, tagging can reveal how the contribution of unmitigated sources to ozone changes in response to mitigation measures (Mertens et al., 2018). Butler et al. (2018) have also noted that tagging studies provide useful diagnostic information about model processes, and argued for their inclusion in model inter-comparison exercises.

125 The method described by Butler et al. (2018) is currently the only available approach which provides separate attribution of tropospheric ozone to its NO_x and reactive carbon precursors.



In this study we use the ozone tagging methodology previously described by Butler et al. (2018) to perform a source attribution for ground-level ozone to both NO_x and reactive carbon. This work builds on the work of Butler et al. (2018) by tagging anthropogenic emissions of NO_x and reactive carbon by their geographical source region, and examining the seasonal cycle of the surface ozone attribution in receptor regions as defined in the HTAP Phase 2 exercise. By performing separate attribution of ground-level ozone to both NO_x and reactive carbon (including methane), we hope to provide more useful information to inform emission mitigation scenarios. We also show how our tagging methodology can be used as a model diagnostic tool to understand the atmospheric budgets of ozone and PAN in more detail than previously possible, potentially informing efforts to reduce the currently high level of inter-model uncertainty. Furthermore, we examine the changing contributions of the different sources of NO_x and reactive carbon to a perturbation of the global methane burden, showing how the contribution of emissions from unmitigated sectors would respond to mitigation of methane emissions.

The tagging approach and model setup is described in Section 2. In Section 3 we evaluate our simulations against observations from TOAR and the ensemble of simulations from HTAP Phase 2, show the intercontinental source attribution for ozone and its precursors, and examine the response of this source attribution to a 20% perturbation in the global methane burden. Conclusions are drawn in Section 4.

2 Experiment design

Simulations are performed with CAM4-chem (Community Atmosphere Model version 4 with chemistry), a component of the CESM (the Community Earth System Model) version 1.2.2 (Tilmes et al., 2015; Lamarque et al., 2012) using the same model configuration as Butler et al. (2018). The model is run at a horizontal resolution of 1.9×2.5 degrees, with 56 vertical levels using specified dynamics for the year 2010 from the MERRA reanalysis (Rienecker et al., 2011). As in Butler et al. (2018), we have replaced the default chemical mechanism with a tagged mechanism based on an earlier version of the MOZART-4 mechanism Emmons et al. (2012). Our tagging system allows the attribution of tropospheric ozone to chemical production by either NO_x or reactive carbon precursors (as well as transport from the stratosphere). A complete attribution of tropospheric ozone to both kinds of precursors requires two model runs: one with NO_x emissions tagged; and another with reactive carbon emissions tagged. Chemical production of ozone in the stratosphere (primarily through photolysis of molecular oxygen), and other minor production pathways for tropospheric ozone are also tagged, as described in Butler et al. (2018). For both NO_x tagging and VOC tagging, the sum of the tagged ozone tracers is equal to the total ozone as simulated by the model.

As in Butler et al. (2018), anthropogenic emissions of NO_x , CO, and NMVOC for 2010 are taken from the EDGAR-HTAPv2 emission inventory (Janssens-Maenhout et al., 2015), biomass burning emissions are from GFEDv3 (van der Werf et al., 2010), and methane is held fixed at the surface to a global average value of 1760 ppb. Two simulations (base runs) are performed with this model setup: one in which all sources of NO_x are tagged as described below (the “ NO_x -tagged” run); and one in which all sources of reactive carbon are tagged as described below (the “VOC-tagged” run). As in Butler et al. (2018), the length of the spinup period was one year for the NO_x -tagged run, and two years for the VOC-tagged run.



160 With the exception of surface-based anthropogenic emissions of NO_x , CO, and NMVOC, the tag identities used in this study
are identical to those used in Butler et al. (2018). In this study, all surface-based anthropogenic emissions are tagged with a label
representing the geographical location at which the emissions occur. This approach allows attribution of simulated ozone to
anthropogenic precursor emissions from specific locations. Specifically, anthropogenic emissions of NO_x and reactive carbon
are tagged according to their Tier 1 Source Region as defined for the HTAP phase 2 multi-model ensemble experiment, which
165 is described in more detail in (Galmarini et al., 2017). Due to computational constraints, not all of the HTAP Tier 1 regions
are tagged in this study. Since the primary focus of this study is on the attribution of ground-level ozone in the Northern
Hemisphere, only the major anthropogenic Northern Hemisphere source regions are tagged, while other anthropogenic sources
are tagged with the label “Rest of the World”. A full list of the tags used in the NO_x - and VOC-tagged runs is given in
Table 1. The explicitly tagged source regions differ between the NO_x -tagged and VOC-tagged runs because VOC tagging
170 is computationally more expensive than the NO_x -tagging (Butler et al., 2018). One important difference between this study
and Butler et al. (2018) is that anthropogenic emissions of CO for each source region are tagged together with emissions of
NMVOC in this study in order to save computational resources.

In addition to the NO_x - and VOC-tagged base runs described above, we also perform two additional runs in order to
investigate the response of tropospheric ozone to a perturbation in the tropospheric burden of methane: one with NO_x tagging;
175 and another with VOC tagging. In each of these methane perturbation runs, the initial atmospheric methane burden and the
methane mixing ratio imposed at the surface as a boundary condition are reduced by 20%. This translates to a surface methane
mixing ratio of 1410 ppb in these methane perturbation runs. In these methane perturbation runs, all other sources of NO_x and
reactive carbon are left unchanged. The methane perturbation runs also require two years of spinup for the model to arrive at
steady state.

180 CAM4-chem in version 1.2.2 of the CESM has previously been evaluated by Tilmes et al. (2015), and the modified version
used in this study has also been discussed thoroughly by Butler et al. (2018). In Section 3, we describe the key differences in
methane and tropospheric ozone between our base simulation and the CAM4-chem simulation reported by Tilmes et al. (2015),
and compare our simulated surface ozone with observations from TOAR (Schultz et al., 2017) as well as with the ensemble
of CTM simulations from the HTAP phase 2 multi-model study (Galmarini et al., 2017). The full set of CTMs participating
185 in the HTAP phase 2 multi-model ensemble is given in Table 3 of Galmarini et al. (2017). In this study we compare surface
ozone from our base simulation with results from a subset of twelve CTMs: CAM-chem (simulations performed by NCAR);
CHASER_re1; CHASER_t106; C-IFS; C-IFS_v2; EMEP_rv4.5; EMEP_rv48; GEMMACH; GEOS-Chem-ADJOINT; GEOS-
Chem; OsloCTM3.v2; RAQMS. Details of the configurations used by each of these models in the HTAP phase 2 ensemble can
be found in Galmarini et al. (2017), and references therein.

190 3 Results and discussion

All results presented in this study are based on the definition of the troposphere as the model grid cells below the level of 150
ppb of ozone. By design, the ozone simulated in our base model runs is identical with the simulation reported in Butler et al.



(2018). Our simulation for 2010 produces a tropospheric ozone burden of 319 Tg(O₃), which is within one standard deviation of the multi-model mean reported by Young et al. (2013) for the year 2000 (337 ± 23 Tg(O₃)). Our simulated tropospheric ozone burden is slightly higher than the burden reported by Tilmes et al. (2015) using a similar model setup (309 Tg(O₃)), which could be due to the use of different emissions datasets. Our simulated tropospheric methane burden (4150 Tg(CH₄)) is the same as reported by Tilmes et al. (2015), but our methane lifetime (due to oxidation in the troposphere by OH), at 7.59 years, is shorter than the 8.82 years reported by Tilmes et al. (2015), likely also due to the use of different emission datasets. Our methane lifetime is towards the lower end of the range (7.1 – 10.6 years) simulated in CTMs, as reported by Saunio et al. (2016).

In Figure 1 we compare our simulated monthly mean surface ozone mixing ratio for 2010 with data from TOAR and with the other models in the HTAP phase 2 CTM ensemble. Results are shown averaged over HTAP Tier 2 receptor regions, and only include grid cells for which TOAR observations are available. In general, most of the HTAP models overestimate the monthly mean surface ozone mixing ratio in regions for which observations are available, consistent with the high model bias reported by Young et al. (2018). Also apparent from Figure 1 is the large range in simulated surface ozone between members of the HTAP model ensemble, which is especially high in the northern spring, approaching a spread of approximately 30 ppb between the lowest and highest ensemble members. Our modelled monthly average surface ozone mixing ratio in the HTAP Tier 2 receptor regions is generally close to the HTAP ensemble mean, and usually within one standard deviation of the ensemble mean.

3.1 Source attribution of tropospheric ozone

The attribution of annual average tropospheric ozone to emissions of NO_x and reactive carbon precursors based on the source tags from Table 1 is shown in Figures 2 and 3 and quantified in Tables 2 and 3. Figures showing the attribution of monthly mean ozone are available in the Supplementary Material. For each tagged source, Tables 2 and 3 include the emissions of NO_x and reactive carbon (respectively, and where applicable), the contribution of each source to the 2010 average tropospheric ozone burden, the contribution to the Northern Hemisphere 2010 annual average surface mixing ratio, and (where applicable) the ozone production efficiency of each emission source (in moles of ozone produced per mole of N or C emitted). Figures 2 and 3 show the spatial distribution of the annual average surface ozone as attributed to each source of NO_x and reactive carbon, respectively. In Figure 2, ozone attributable to anthropogenic NO_x emissions in some source regions has been added to the “Rest of the world” total in order to unify the definition of this source region with the definition of this region in the VOC-tagged run. The difference in the stratospheric contribution between the NO_x- and VOC-tagged runs is due to the role of NO_x produced in the stratosphere from dissociation of N₂O. Ozone produced in reactions involving this stratospheric source of NO_x are counted in our source attribution as stratospheric ozone, as described in Butler et al. (2018).

3.1.1 Attribution to NO_x emissions

Anthropogenic NO_x emissions from the three major high-latitude source regions (Europe, East Asia, and North America) contribute to high modelled ozone concentrations both locally and in the Northern Hemisphere background. Lightning NO_x,



soil NO_x , and ozone input from the stratosphere all contribute additionally to modelled global background ozone. Emissions of NO_x from shipping contribute significantly to ozone over the major northern hemisphere ocean basins, which is also transported over continental regions. South Asia stands out in comparison with the other major Northern Hemisphere source regions, in that ozone produced from NO_x emitted in South Asia is relatively localised to the South Asian region itself, and not transported into the hemispheric background to the same extent as ozone produced from NO_x emissions in the other major Northern Hemisphere source regions.

Table 2 shows that NO_x emissions from lightning and aircraft are especially efficient at producing ozone in the free troposphere, consistent with previous work (eg. Beck et al., 1992; Jacob et al., 1996). Similarly, surface emissions of NO_x from regions closer to the tropics (eg. South East Asia and Middle America) produce ozone more effectively due to rapid convective transport of emitted NO_x into the free troposphere, consistent with Zhang et al. (2016). Of the major Northern Hemisphere source regions, NO_x emissions from South Asia are the most efficient at producing ozone, consistent with a stronger role of vertical transport over this region. In contrast, NO_x emissions from the major anthropogenic source regions in the high northern latitudes (Europe, East Asia, and North America) are among the least productive of all global NO_x emissions, consistent with a relatively small amount of convective transport, leading to higher rates of NO_x removal. Despite their low ozone production efficiency, emissions of NO_x in the high northern latitudes contribute significantly to surface ozone across the northern hemisphere (Figure 2 and Table 2).

Table 2 also shows that NO_x emissions from shipping are also relatively efficient at producing ozone, which is also consistent with previous work (eg. Lawrence and Crutzen, 1999; Hoor et al., 2009). The high ozone production efficiency of ship emissions is due to their location in relatively pristine regions with few other sources of NO_x . Due to the high ozone productivity of ship emissions, and being emitted at relatively high latitudes, they contribute significantly to the Northern Hemispheric background (Figure 2 and Table 2). As noted above, the ozone production from ship NO_x is likely to be overestimated due to the artificial dilution of emissions into relatively coarse model grid cells.

Mertens et al. (2018) report a contribution of shipping to the tropospheric ozone burden of 18 $\text{Tg}(\text{O}_3)$ using their tagging technique, and based on a model simulation with ship NO_x emissions of 6 $\text{Tg}(\text{N})\text{yr}^{-1}$. In our study, we calculate a contribution of ship NO_x to tropospheric ozone of 19.9 $\text{Tg}(\text{O}_3)$ based on ship NO_x emissions of 4.28 $\text{Tg}(\text{N})\text{yr}^{-1}$, implying a much higher ozone production efficiency for ship NO_x in our study. Since the tagging technique used by Mertens et al. (2018) is based on the technique described by Grewe et al. (2017), which combines the effects of tagged NO_x and reactive carbon precursors into a single tagged ozone molecule during ozone production, we do not expect our results to be directly comparable. Since shipping emits significantly more NO_x than reactive carbon, we would expect the combinatorial tagging approach of Mertens et al. (2018) to attribute less ozone to shipping than our method, as the ozone produced from ship NO_x would also be partially attributed to the reactive carbon precursor involved in the ozone production. Indeed, Mertens et al. (2018) report maximum contributions of shipping to surface ozone of about 10 ppb in summer over major Northern Hemisphere ocean basins. In our study, surface ozone attributable to shipping over these regions can exceed 20 ppb (see the Supplementary Material).



3.1.2 Attribution to reactive carbon emissions

260 Methane and biogenic emissions clearly stand out as major reactive carbon precursors to tropospheric ozone, contributing 35% and 24% respectively to the tropospheric ozone burden in our simulation. Anthropogenic emissions of reactive carbon (excluding biomass burning) together contribute about 14 % to the tropospheric ozone burden. The relatively low influence of anthropogenic reactive carbon emissions on ground-level ozone has been noted elsewhere (eg. HTAP, 2010; Butler et al., 2018), but despite this low overall ozone productivity, anthropogenic reactive carbon emissions from source regions in higher
265 northern latitudes still contribute disproportionately highly to surface ozone in the Northern Hemisphere (Table 3).

Due to the emissions of CO being tagged together with emitted VOC in this study, the contribution of each tagged source to the tropospheric ozone burden (and therefore also the ozone production efficiency of each tagged source) is a mixture of ozone production due to emitted CO and emitted NMVOC. The ozone attributed to methane oxidation in Table 3 is due do all stages of methane oxidation in the MOZART-4 chemical mechanism, including the final step in which CO from earlier
270 stages of methane oxidation is itself oxidised to CO₂. The oxidation of CO can produce at maximum one peroxy radical (HO₂). The maximum ozone production potential of CO is therefore 1 mole of ozone per mole of emitted CO. VOC (including methane) can produce significantly more ozone per mole emitted carbon, when taking into account the subsequent oxidation of the initial oxidation products (Butler et al., 2011). Future studies using this tagging methodology should consider tagging
275 CO emissions separately from NMVOC emissions if they aim to determine the ozone production efficiency of anthropogenic NMVOC emissions from different world regions. Butler et al. (2018) did tag NMVOC emissions separately from CO emissions, but did not tag anthropogenic emissions separately according to their geographical region. We reexamined the output of the otherwise identical VOC-tagged run described by Butler et al. (2018) in order to determine the ozone production efficiency of NMVOC emissions from anthropogenic, biomass burning, and biogenic sources. Respectively, these are 0.0580, 0.0354, and 0.0268 (mol(O₃)/mol(C)). The ozone production efficiency of biogenic NMVOC recalculated from Butler et al. (2018) is
280 not significantly different from the value reported here in Table 3, reflecting the relative minor contribution of CO to the total amount of emitted biogenic reactive carbon. For biomass burning and anthropogenic sources however, the ozone production efficiency of NMVOC emitted from these sources is greater than the corresponding value from Table 3, reflecting the fact that the numbers from Table 3 also include emissions of CO.

Interestingly, we note that methane has a higher ozone production efficiency (0.0689 mol mol⁻¹, Table 3) than any of the
285 NMVOC in our runs. The low ozone production efficiency of biogenic NMVOC is consistent with large amounts of isoprene being emitted in remote regions under low-NO_x conditions, where loss of peroxy radicals through reaction with other peroxy radicals could be expected to dominate (Atkinson, 2000). It might however be expected that anthropogenic NMVOC would have a higher ozone production efficiency, due to their being co-emitted with anthropogenic NO_x, favouring the conversion of NO to NO₂ through reaction with peroxy radicals, and thus the production of ozone. The relatively low production efficiency
290 of anthropogenic NMVOC in our model runs could be due to the relatively simple chemistry of methane oxidation being well-described in the version of the MOZART-4 chemical mechanism used here, in which the relatively complex chemistry of the higher NMVOC has been simplified. Coates and Butler (2015) noted that the ozone production potential of NMVOC



in simplified chemical mechanisms tended to be lower than the more comprehensive Master Chemical Mechanism (Saunders et al., 2003). Utembe et al. (2010) previously noted increased tropospheric ozone in a CTM when using a more explicit
295 oxidation mechanism for NMVOC. The extremely low ozone production efficiency of reactive carbon from oceanic sources in Table 3 is due to the lack of any ozone forming pathways in the oxidation of dimethyl sulphide (DMS) in the MOZART-4 chemical mechanism as used in this study. DMS is the dominant source of reactive carbon over the oceans in our model simulations.

To our knowledge, the only other study to perform source attribution of global tropospheric ozone specifically to reactive
300 carbon precursors is Butler et al. (2018), on which the present study builds. Here, we attribute 113 Tg of ozone to methane oxidation (Table 3). Grewe et al. (2017) attribute 45 Tg of ozone to methane using their tagging approach, which combines the effects of tagged NO_x and reactive carbon precursors into a single tagged ozone molecule during ozone production. Ozone production due to methane oxidation under their combinatorial tagging approach would be expected to also include attribution to the source of NO_x involved in the ozone production. We would thus expect Grewe et al. (2017) to attribute approximately
305 half of the amount of ozone to methane as we would. Doubling the value reported by Grewe et al. (2017) yields 90 Tg of ozone attributable to methane oxidation, which is much closer to our value of 113 Tg.

Widespread implementation of tagging techniques for separated tagging of NO_x and reactive carbon emissions in other CTMs, along with systematic inter-comparisons of their results could help to understand differences in the simulated budgets of tropospheric ozone.

310 3.2 Source-receptor relationships for ozone

3.2.1 Annual average surface ozone

Figure 4 shows the modelled annual average surface ozone concentration in the five major HTAP Tier 1 regions in the northern hemisphere (Europe, Russia/Belarus/Ukraine, South Asia, East Asia, and North America), including a full attribution of ozone in each of these regions to all sources, including transport from the stratosphere and emitted precursors of both NO_x and
315 reactive carbon. Annual average ozone in most of the regions shown in Figure 4 is close to the Northern Hemisphere annual average of 30 ppb (Table 2), except in South Asia and East Asia, where the annual average surface ozone mixing ratio is closer to 40 ppb. The difference in each case is primarily due to a larger source of ozone produced from locally emitted precursors. Transport from the stratosphere contributes approximately 2–4 ppb to annual average surface ozone depending on the receptor region, consistent with the 2.91 ppb contribution of stratospheric ozone to the annual average surface ozone in
320 the Northern Hemisphere average surface ozone (Table 3). As already shown in the previous section, anthropogenic sources of NO_x dominate other NO_x sources as ozone precursors, while the major reactive carbon precursors are methane and BVOC.

In each of the five regions shown in Figure 4, natural sources and long-range transport of ozone produced from extra-regional anthropogenic precursors contribute more to the annual average surface ozone than anthropogenic emissions within the region itself. In each region, the local anthropogenic NO_x emissions produce more ozone than can be attributed to anthropogenic
325 NO_x emissions in any other Tier 1 regions, but with only one exception (South Asia), the combined contribution of external



anthropogenic NO_x emissions to annual average surface ozone is greater than the local contribution. The importance of long-range transboundary transport of ozone has been noted elsewhere (HTAP, 2010).

While anthropogenic precursor emissions from South Asia contribute significantly to surface ozone within the South Asia region, they contribute relatively little to surface ozone in the other four regions shown in Figure 4. This is also consistent with the surface ozone maps in Figure 2, and the higher ozone productivity of NO_x emissions from South Asia when compared with the other major Northern Hemisphere source regions (Table 2). Emissions of ozone precursors (particularly NO_x) from South Asia are transported efficiently into the free troposphere, where they contribute disproportionately to the global tropospheric ozone burden (as also noted by Zhang et al., 2016), but the contribution of South Asian emissions to surface ozone in other parts of the Northern Hemisphere is disproportionately smaller than emissions from the other HTAP Tier 1 regions.

3.2.2 Seasonal cycles of surface ozone

Figures 5, 6, and 7 show the seasonal cycles of surface ozone in the three selected Tier 2 regions “North West Europe”, “North East China”, and “North West United States” respectively. A set of figures for other HTAP Tier 2 regions, with a complete attribution of surface ozone to all tagged HTAP Tier 1 source regions is available in the Supplementary Material. In each of Figures 5, 6, and 7, results are shown for both NO_x - and VOC-tagging. In each receptor region, the contribution of long-range transport due to extra-regional anthropogenic emissions from HTAP Tier 1 regions is shown both in aggregate (top panels) and by individual Tier 1 source region (bottom panels). The definition of the “Rest of the world” ozone tracer has been harmonised between the NO_x - and VOC-tagged runs in these figures. Consistent with the annual averages from Figure 4, anthropogenic NO_x sources also dominate the seasonal cycle of modelled ozone, while the major reactive carbon precursors of ozone are methane and BVOC.

All three receptor regions show a seasonal cycle of ozone with a spring-summer ozone maximum superimposed on a year-round ozone baseline. The summertime maximum in ozone is clearly due to local photochemical production from the combination of locally-emitted anthropogenic NO_x and biogenic VOC. The strong role of locally-emitted precursors in the production of ozone in summer is consistent with earlier work (eg. Reidmiller et al., 2009; Huang et al., 2017; Jonson et al., 2018; Han et al., 2019), while the importance of biogenic VOC emissions, especially isoprene, for ozone production in summer has also been noted elsewhere (eg. Chameides et al., 1992; Andersson and Engardt, 2010; Han et al., 2019). Biogenic emissions of NO_x (from soils) also contribute to this summertime maximum in local photochemical ozone production in all three of the regions shown in Figures 5, 6, and 7, but to a much smaller extent than anthropogenic NO_x emissions.

The year-round baseline ozone in our model simulations in all three receptor regions can be primarily explained by slower photochemistry involving methane as the reactive carbon precursor, in combination with extra-regional anthropogenic NO_x (Figures 5, 6, and 7). Both show a minimum contribution in winter of about 10 ppb in all three receptor regions. The contribution of methane to surface ozone is slightly larger in summer, coinciding with the peak in local anthropogenic NO_x emissions, consistent with local photochemical ozone production from enhanced local methane oxidation. The contribution of extra-regional anthropogenic NO_x to surface ozone is largest in spring, coinciding with the peak in the contribution of extra-regional anthropogenic reactive carbon, consistent with long-range transboundary transport of ozone produced elsewhere.



360 Maxima in springtime ozone have previously been linked to long-range transboundary transport in all major receptor regions (HTAP, 2010; Lin et al., 2012; Jonson et al., 2018; Ni et al., 2018). This transported ozone can be attributed to input from the stratosphere, as well as extra-regional anthropogenic emissions of NO_x and reactive carbon. In our simulations, the contribution of stratospheric ozone peaks around March, while the contribution of extra-regional anthropogenic emissions tends to peak around April, when it contributes more strongly to monthly average surface ozone in each region than local anthropogenic NO_x (Figures 5, 6, and 7). In all regions, the springtime peak in the contribution of extra-regional anthropogenic reactive carbon is smaller, but more pronounced than the corresponding springtime peak in the contribution of extra-regional anthropogenic NO_x . Previous work has identified uncertainties in the treatment of ozone production from NMVOC oxidation as a potential source of inter-model differences (eg. Emmerson and Evans, 2009; Utembe et al., 2010; Coates and Butler, 2015). The relatively large influence of anthropogenic NMVOC on springtime ozone (compared with its influence during other time of the year) could be a contributing factor to the large spread in springtime ozone simulated by current generation CTMs (Figure 1).

NO_x from shipping is the largest single contributor to springtime transboundary ozone transport in all three receptor regions shown here. We note however that the coarse resolution of our model (2 degrees) would be expected to exaggerate the effects of ship NO_x on ozone production due to rapid dilution of the emissions (von Glasow et al., 2003), as well as exaggerate the transport of NO_x and ozone near coastlines due to unrealistically high diffusion between adjacent land and ocean grid cells. The contribution of shipping emissions to surface ozone in our simulations should thus be considered an upper bound, especially in coastal regions. The high contribution of ship NO_x to summertime ozone in Europe (Figure 5) may be an artefact of coarse model resolution, combined with high shipping volume near coasts in the Eastern North Atlantic Ocean as well as the North Sea. Early work by Lawrence and Crutzen (1999) showed a stronger influence of ship NO_x on surface ozone in North West Europe than on any other continental region. Jonson et al. (2018) show that the only other CTM in the HTAP phase 2 ensemble to report the results of a perturbation of shipping emissions (the EMEP_rv48 CTM with a resolution of 0.5×0.5 degrees) shows a similar magnitude for the influence of ship NO_x on summertime ozone in Europe as for springtime ozone. Lupaşcu and Butler (2019), using a regional model at 50×50 km resolution and a similar ozone tagging system as used in the present study, showed that the contribution of ship NO_x to ozone in coastal regions of Europe reaches a maximum level in summer. Jonson et al. (2020), using a global model with a resolution of 0.5×0.5 degrees showed that shipping near coastal regions contributes significantly to ozone over North West Europe in both spring and summer, while NO_x emissions from shipping on the high seas makes a stronger contribution to European ozone in spring than in summer. In contrast, the study of Aksoyoglu et al. (2016), using a higher-resolution regional model (20×20 km) for Europe, does not indicate such a strong role for ship NO_x on summertime ozone over Europe.

In other receptor regions, the influence of ship NO_x emissions on surface ozone is largest in spring (Figures 6 and 7), suggesting a stronger influence of NO_x emissions over the high seas on springtime ozone in our simulations in these regions. Model-dependent inconsistencies in the treatment of ship NO_x emissions may play a role in the large spread of simulated ozone between models in springtime (Figure 1). Future work should examine the contribution of ship NO_x emissions to ozone in both spring and summer, using model systems which include both better representations of plume dilution over the major shipping routes, and higher resolution over receptor regions.



395 Previous work has indicated a strong influence of anthropogenic emissions from both North America and East Asia on
springtime ozone in Europe (Jonson et al., 2018), a strong influence of East Asian emissions on springtime ozone in North
America (Lin et al., 2012), and a diverse range of intercontinental influences on springtime ozone in East Asia (Ni et al., 2018).
Direct numerical comparison of our results with these previous studies is difficult due to the different methodologies used.
These previous studies all employed the perturbation technique to determine the influence of all anthropogenic emissions (both
400 NO_x and reactive carbon) from each source region, while this work uses a tagging approach which separately attributes ozone
to emitted NO_x and reactive carbon. Qualitatively, our results as shown in Figures 5, 6, and 7 do however appear consistent
with this earlier work. Comparison of the NO_x -tagged and VOC-tagged results in these Figures shows that anthropogenic
 NO_x emissions from most source regions have a stronger influence on springtime ozone in any given receptor region than
anthropogenic emissions of reactive carbon. The only exception to this is East Asia, where reactive carbon emissions are
405 substantially higher than in other HTAP Tier 1 source regions (Table 3). Reactive carbon emissions from East Asia contribute
approximately equally to springtime ozone in North America as East Asian NO_x emissions, and in Europe, East Asian reactive
carbon contributes more to springtime ozone than East Asian NO_x .

3.3 Long-range transport of ozone precursors

Fiore et al. (2018) has suggested that measurements of the abundance of PAN at mountaintop sites in spring may be useful as
410 an indicator of intercontinental transport of ozone and its precursors, as well as being a diagnostic for uncertainties in CTM
simulations, which show large inter-model differences in simulated PAN (Emmons et al., 2015). The column integrated density
of PAN in the lower troposphere (defined here as the model layers between 500 and 800 hPa) in the three HTAP Tier 2 receptor
regions “North West Europe”, “North East China”, and “North West United States” are shown in Figures 8, 9, 10. A set of
figures for other HTAP Tier 2 regions, with a complete attribution of surface ozone to all tagged HTAP Tier 1 source regions
415 is available in the Supplementary Material. Simulated PAN is highest in late winter to early spring, consistent with earlier
work (Fischer et al., 2014; Fiore et al., 2018). The extra-regional contribution to PAN is also highest in spring, and this is due
primarily to anthropogenic NMVOC, also consistent with Fischer et al. (2014).

Our model simulations with NO_x - and VOC tagging provide a unique opportunity to examine the origin and fate of PAN
as simulated in our model, since this allows simultaneous attribution of simulated PAN to both is NO_x precursor and its
420 reactive carbon precursor. Comparison of the bottom two panels in each of Figures 8, 9, 10 shows consistently that for any
given land-based HTAP Tier 1 source region, the anthropogenic NMVOC emissions contribute more to PAN formation than
the anthropogenic NO_x emissions from that region to the PAN modelled in all HTAP Tier 2 receptor regions. The balance
of extra-regional PAN in all cases is due to NO_x emissions from shipping. In our simulations, significant amounts of PAN
are formed downwind of the regions in which the anthropogenic NMVOC precursors are emitted, often through reaction with
425 NO_x emitted from shipping. A strong influence of anthropogenic NO_x emissions on PAN in the northern mid-latitudes is
consistent with the results shown by Fischer et al. (2014) (their Figure 7, which does not distinguish between different sources
of anthropogenic NO_x).



Figures 8, 9, and 10 also show that the reactive carbon component of PAN is generally more persistent than the NO_x component. For example, the contribution of anthropogenic NMVOC from North America to springtime PAN over East Asia is only slightly lower than its contribution to springtime PAN over Europe, which is much closer to North America considering the prevailing westerly winds (bottom right panels of Figures 8 and 9). In contrast, the contribution of anthropogenic NO_x from North America to springtime PAN in East Asia is substantially less than its contribution to springtime PAN over Europe (bottom left panels of Figures 8 and 9).

We examine the Northern Hemisphere budget of reactive carbon in more detail in Figure 11. This figure shows the seasonal cycle of the Northern Hemisphere column-integrated total reactivity with respect to the OH radical of all reactive carbon containing species in our simulation, attributed to their emission source. The total OH reactivity of reactive carbon species of an air mass is often linked to its ozone production potential (Chameides et al., 1992; Kleinman et al., 2002). The OH reactivities shown in Figure 11 include in each case the OH reactivity of the primary emitted species, as well as the OH reactivity of each carbon-containing oxidation product. These were calculated using monthly averaged output of the modelled concentration of each carbon-containing species (including its associated tags), and the temperature- and pressure-dependent rate coefficients for their reaction with the OH radical, then averaged over all Northern Hemisphere grid cells, weighted by air density.

The total Northern Hemisphere OH reactivity of reactive carbon remains fairly constant year-round at about $0.6 - 0.7 \text{ s}^{-1}$, but the seasonal cycles of the OH reactivity attributable to different reactive carbon sources show more variability. Methane (and its oxidation products) contribute about $0.2 - 0.3 \text{ s}^{-1}$ (almost half of the total hemispheric reactivity), with a slight maximum in the summer, consistent with enhanced oxidation (and thus enhanced availability of more reactive methane oxidation products) due to higher OH in summer. The contributions of anthropogenic and biogenic reactive carbon sources to total hemispheric reactivity are similar, ranging between about $0.1 - 0.3 \text{ s}^{-1}$, but with distinct seasonal cycles. The reactivity of biogenic carbon is highest in summer-autumn (consistent with the Northern Hemisphere growing season), while reactivity of anthropogenic carbon is highest in winter-spring (consistent with constant year-round anthropogenic emissions, and a build-up of reactive carbon over winter due to lower hemispheric OH). The build-up of anthropogenic reactive carbon throughout the Northern Hemisphere over winter, combined with the resumption of OH chemistry in spring is consistent with the disproportionate effect of extra-regional anthropogenic reactive carbon on springtime ozone seen in Figures 5, 6, and 7. Uncertainties in the model chemical mechanisms associated with the oxidation of anthropogenic NMVOC (eg. Emmerson and Evans, 2009; Utembe et al., 2010; Coates and Butler, 2015) may thus also contribute to the large spread in simulated ozone seen in the HTAP ensemble during spring (Figure 1).

Figure 11 also shows the geographical origin of Northern Hemisphere anthropogenic carbon reactivity. Emissions of reactive carbon from East Asia stand out as the single major source of enhanced anthropogenic carbon reactivity in winter and spring in our simulations. This is consistent with the high emissions of reactive carbon from this region in 2010 noted earlier (Table 3). Growth in NMVOC emissions from East Asia may have continued since this time (Li et al., 2019), while NO_x emissions have been decreasing (Liu et al., 2017). Increasing trends in local production of ozone during summer over East Asia (eg. Li et al., 2018) should be associated with increased oxidation of reactive carbon, and thus potentially less export of reactive carbon into the Northern Hemisphere background during summer. We expect, however, that increasing emissions of reactive carbon in East



Asia should lead to an increased build-up of East Asian reactive carbon in the Northern Hemisphere over winter, and thus also to increased East Asian contribution to extra-regional springtime ozone in other parts of the Northern Hemisphere.

465 Our tagging technique is currently the only one we know of which is capable of examining the budget of reactive carbon in the level of detail presented in this study. The separate tracking of the carbon-containing and nitrogen-containing components of PAN is particularly informative, suggesting that significant amounts of PAN are formed downwind of source regions in our model, especially during winter and spring, due to a build-up of anthropogenic reactive carbon over winter when photochemistry is relatively slow. Given the large variety in model representations of NMVOC chemistry, including PAN formation and
470 decomposition processes (Emmerson and Evans, 2009; Knote et al., 2015) and the large inter-model differences in simulated PAN (Emmons et al., 2015), the widespread implementation of similar tagging diagnostics in other CTMs may help to provide additional information about the origin and fate of simulated PAN, and more generally about the influence of reactive carbon on atmospheric composition. In combination with routine mountaintop observations of springtime PAN, this may aid understanding of the global PAN budget (Fiore et al., 2018) and other processes responsible for intercontinental transport of
475 air pollution. Better constraints on these chemical and transport processes should also help to reduce inter-model differences in simulated springtime ozone (Figure 1).

3.4 Tropospheric ozone sensitivity to methane

We performed an additional set of model runs with both NO_x - and VOC-tagging with the methane surface boundary condition reduced from 1760 ppb to 1410 ppb, a reduction of 350 ppb, or 20%. This perturbation can also be expressed as an increase of
480 25%. Here we interpret the methane perturbation run in terms of the atmospheric response to a 25% increase in the methane surface mixing ratio at steady state.

In response to the 25% increase in the imposed surface mixing ratio of methane, the total tropospheric burden increased by 776 $\text{Tg}(\text{CH}_4)$, an increase of 23%. The strength of the annual tropospheric chemical sink of methane due to OH increased by 72.5 $\text{Tg}(\text{CH}_4)$, or 15.2%. The corresponding increase in the methane lifetime was 0.48 years, or 6.75%. The relatively small
485 growth in the chemical methane sink compared with the magnitude of the perturbation in methane itself is consistent with the feedback of methane on its own lifetime due to depletion of OH (Prather, 1996). Table 4 shows the response of the tropospheric ozone burden (and the contributions of different reactive carbon precursors) to the 25% increase in the imposed surface mixing ratio of methane. The 1 ppb simulated increase in Northern Hemisphere surface ozone in response to a 25% increase in methane burden is consistent with previous work (HTAP, 2010). The 9.22 Tg increase in tropospheric ozone burden is also consistent
490 with the review of Fiore et al. (2008), who derived a sensitivity of 0.11–0.16 $\text{Tg}(\text{O}_3)$ per $\text{Tg}(\text{CH}_4)\text{yr}^{-1}$ emitted based on an analysis of the literature. We calculate 0.13 $\text{Tg}(\text{O}_3)$ per $\text{Tg}(\text{CH}_4)\text{yr}^{-1}$ based on our results.

The relative increase in tropospheric ozone due to methane (13.0%) is comparable to, but slightly smaller than the increase in the magnitude of the chemical methane sink due to OH (15.2%), consistent with the troposphere as a whole becoming slightly more NO_x -limited with increasing methane. The relative increase in the total ozone burden (2.98%) is, however,
495 significantly lower than the increase in the ozone produced from methane oxidation. When the methane burden is increased, the contribution of every other reactive carbon source to the tropospheric ozone burden decreases (each by approximately 1



– 2%) to partially offset the increased ozone production from methane oxidation. This is also consistent with a slightly more NO_x -limited atmosphere with increasing methane. In a future with an increased methane burden, control of NMVOC emissions could be expected to be less effective at large-scale reduction in ground-level ozone.

500 Table 5 shows the change in the contributions of different NO_x sources to tropospheric ozone in response to the 25% increase in methane burden. As expected, all NO_x sources become more productive when the total atmospheric burden of reactive carbon is increased (consistent with the troposphere as a whole becoming more NO_x -limited). The increase in the productivity of the different NO_x sources under an increased burden of methane is however not uniform. Ozone production due to NO_x from shipping stands out as highly sensitive to the global methane burden in our simulations. Ship NO_x accounts
505 for almost 30% of the 1 ppb increase in Northern Hemisphere average surface ozone when the methane burden is increased by 25% (Table 5), despite being a much smaller percentage of total global NO_x emissions (Table 2).

The spatial distribution of the increase in annual average surface ozone from ship NO_x in response to the 25% increase in methane is similar to the spatial distribution of surface ozone due to ship NO_x in our base run (Figure 2). Figures showing the response of attributed surface ozone are available in the Supplementary Material. The response is largest over the major
510 Northern Hemisphere ocean basins, but also extends over continental regions. The seasonal cycle of the increase in annual average surface ozone from ship NO_x in the three HTAP Tier 2 regions examined here in response to the 25% increase in methane is similar to the seasonal cycle of surface ozone due to ship NO_x in our base run (Figures 5, 6, and 7). The maximum response of surface ozone from ship NO_x to rising methane is simulated over the major Northern Hemisphere ocean basins in summer (which in our simulations influences surface ozone in North West Europe, Figure 5), while the influence of this
515 response over most Northern Hemisphere continental regions is generally higher in winter-spring (as seen in North East China, Figure 6).

Previous work (Lawrence and Crutzen, 1999) has noted the disproportionate influence of ship NO_x on tropospheric ozone due to the diffuse and widespread nature of this source over regions which would otherwise have very low mixing ratios of NO_x . Fiore et al. (2008) noted that the response of surface ozone to increased methane was especially strong in ship tracks.
520 Myhre et al. (2011) also showed that ship NO_x emissions reduce the global methane lifetime much more than terrestrial NO_x emissions. We note again that the contribution of ship NO_x to ozone in our simulations (as in most current-generation CTMs) is likely to be an overestimate due to the unrealistic dilution of these emissions into coarse model grid cells (von Glasow et al., 2003), and the lack of explicit plume chemistry (Vinken et al., 2011). We do expect however, that the interaction between ship NO_x and methane for ozone production would persist in our model even with a more realistic treatment of ship emissions, since
525 this interaction is likely due to the location, rather than the magnitude of ship emissions. We are not aware of any previous work linking the combined influence of these two sources to a potentially disproportionate influence on background ozone in the Northern Hemisphere, and on modelled surface ozone air quality in inhabited regions of the Northern Hemisphere, especially in spring. Given the current uncertainty in attribution of recent trends in methane (Turner et al., 2019) and the potential for future increases in methane emissions, combined with slower reductions in NO_x emissions from international
530 shipping than from other sectors (eg. the SSP5 future emission scenario Rao et al., 2017), we expect that model simulations of future background ozone in the Northern Hemisphere, especially during spring, may come to be increasingly influenced



by ozone produced through the interaction of methane and ship NO_x . Future work should investigate the ozone production through interaction of these two sources in more detail.

4 Conclusions

535 We have performed a source attribution for tropospheric ozone in a chemical transport model using a novel technique which separately accounts for the influence of both the emitted NO_x and the emitted reactive carbon precursors on simulated tropospheric ozone. By tagging anthropogenic emissions of NO_x and reactive carbon according to their geographical region we have calculated source/receptor relationships for the Northern Hemisphere. The results of our study are consistent with previous work, and provide a number of important new insights of relevance to both the mitigation of intercontinental transboundary
540 air pollution and ongoing efforts to reduce the uncertainty in the current generation of chemical transport models.

Consistent with previous work, annual average ground-level ozone in all major Northern Hemisphere regions is primarily influenced by extra-regional emissions of both NO_x and reactive carbon. In all cases, local anthropogenic emissions of ozone precursors have a smaller influence on annual average ozone than the combined effect of precursor emissions from the rest of the world. As a reactive carbon precursor, methane contributes 35% of the tropospheric ozone burden, and 41% of the
545 Northern Hemisphere annual average surface mixing ratio, more than any other source of reactive carbon. Our novel tagging methodology also reproduces the well-known dependence of summer ozone maxima on local emissions of anthropogenic NO_x and biogenic reactive carbon, and the enhanced importance of intercontinental transport of ozone from remote anthropogenic sources in spring. Consistent with previous work, we find that emissions of NO_x at low latitudes produce free-tropospheric ozone more effectively due to more efficient vertical transport. We show, however, that NO_x sources at higher northern latitudes
550 have a stronger influence on ground-level ozone, which has a lower radiative forcing but a higher influence human health and ecosystems.

The current generation of chemical transport models has particular difficulty in simulating the intercontinental transport of ozone, as shown by the large spread in ensemble simulations of ground-level ozone during the spring months. We show that our tagging methodology can deliver detailed diagnostic information about the origin and budget of springtime ozone in our model,
555 along with information about the springtime budget of peroxyacetyl nitrate (PAN), which is also associated with springtime long-range transport and ozone production. We show that a substantial proportion of the free-tropospheric PAN simulated by our model in spring is not produced in the polluted boundary layer over the major anthropogenic source regions, but is rather produced in our model downwind of these regions through the interaction of transported anthropogenic reactive carbon and NO_x emitted from international shipping. Reactive carbon of anthropogenic origin (and its oxidation products, including PAN)
560 builds up in our model across the entire Northern Hemisphere during the winter months, and then contributes in our simulations to a short burst of hemispheric-scale ozone production during spring. In all but the most polluted source regions, anthropogenic NMVOC do not make a significant contribution to simulated ground level ozone in any other season but spring.

We showed here that export of anthropogenic reactive carbon from East Asia may be playing a dominant role in contributing to the build up of reactive carbon in the Northern Hemisphere over winter, and thus to the hemispheric-scale production of



565 ground-level ozone in spring. Given the likely lack of recent mitigation in reactive carbon emissions from East Asia, we expect
this effect to be ongoing, and recommend that future work continue investigation of this possibility using updated emission
inventories.

The springtime peak in transported ozone in our model is influenced by the interaction of two processes known to be
especially poorly represented in current models: the chemistry of the intermediate oxidation products of NMVOC; and the
570 emissions of NO_x from international shipping. Furthermore, the response of ground-level ozone to changes in methane also
appears highly sensitive to the treatment of ship NO_x , especially in spring. We believe that our tagging technique could
deliver useful information about the large differences in simulated springtime ozone between current generation models, if
implemented in a larger number of models and used systematically in model inter-comparison exercises. This could potentially
point the way to improved representations of the processes responsible for intercontinental transport of ozone.

575 Improved global chemical transport models are required to inform effective policies aimed at reducing intercontinental
transport of ground-level ozone, a problem which is most urgent in the springtime. In particular, we recommend that developers
of emission inventories and CTMs revisit their representations of anthropogenic NMVOC emissions and associated oxidation
chemistry in order to reduce the uncertainties in modelled springtime ozone. Additionally, more explicit representations of the
 NO_x chemistry of ship exhaust plumes should be prioritised in order to improve the suitability of current models for simulating
580 both intercontinental transport of ozone as well as the response of ozone to changing atmospheric methane.

Code availability. The CESM is maintained by NCAR, and is provided free to the community. The specific modifications made to the model
to enable tagging of ozone production have been described by Butler et al. (2018) and are available in the online supplement to that work,
which is archived and accessible through the following DOI: 10.5194/gmd-11-2825-2018

Author contributions. TB designed the study. Model runs were performed by AL. Analysis of model runs was performed by AL, AN, and
585 TB. TB wrote the paper with input from AL and AN.

Competing interests. The authors declare that they have no competing interests.

Acknowledgements. The authors would like to thank Mark Lawrence, Louisa Emmons, Simone Tilmes, and Terry Keating for numerous
helpful discussions during the preparation of this manuscript.

Financial support. This work was hosted by IASS Potsdam, with financial support provided by the Federal Ministry of Education and
590 Research of Germany (BMBF) and the Ministry for Science, Research and Culture of the State of Brandenburg (MWFK).



References

- Aksoyoglu, S., Baltensperger, U., and Prévôt, A. S. H.: Contribution of ship emissions to the concentration and deposition of air pollutants in Europe, *Atmospheric Chemistry and Physics*, 16, 1895–1906, <https://doi.org/10.5194/acp-16-1895-2016>, 2016.
- Andersson, C. and Engardt, M.: European ozone in a future climate: Importance of changes in dry deposition and isoprene emissions, *Journal of Geophysical Research*, 115, <https://doi.org/10.1029/2008jd011690>, 2010.
- Atkinson, R.: Atmospheric chemistry of VOCs and NO_x, *Atmos. Environ.*, 34, 2063–2101, 2000.
- Beck, J. P., Reeves, C. E., de Leeuw, F. A., and Penkett, S. A.: The effect of aircraft emissions on tropospheric ozone in the northern hemisphere, *Atmospheric Environment. Part A. General Topics*, 26, 17–29, [https://doi.org/10.1016/0960-1686\(92\)90257-1](https://doi.org/10.1016/0960-1686(92)90257-1), 1992.
- Butler, T., Lawrence, M., Taraborrelli, D., and Lelieveld, J.: Multi-day ozone production potential of volatile organic compounds calculated with a tagging approach, *Atmos. Environ.*, 45, 4082 – 4090, <https://doi.org/10.1016/j.atmosenv.2011.03.040>, <http://www.sciencedirect.com/science/article/pii/S1352231011003001>, 2011.
- Butler, T., Lupascu, A., Coates, J., and Zhu, S.: TOAST 1.0: Tropospheric Ozone Attribution of Sources with Tagging for CESM 1.2.2, *Geoscientific Model Development*, 11, 2825–2840, <https://doi.org/10.5194/gmd-11-2825-2018>, 2018.
- Carter, W.: Development of ozone reactivity scales for volatile organic compounds, *J. Air Waste Manage. Assoc.*, 44, 881–899, 1994.
- Chameides, W. L., Fehsenfeld, F., Rodgers, M. O., Cardelino, C., Martinez, J., Parrish, D., Lonneman, W., Lawson, D. R., Rasmussen, R. A., Zimmerman, P., Greenberg, J., Mlddleton, P., and Wang, T.: Ozone precursor relationships in the ambient atmosphere, *Journal of Geophysical Research*, 97, 6037, <https://doi.org/10.1029/91jd03014>, 1992.
- Clappier, A., Belis, C. A., Pernigotti, D., and Thunis, P.: Source apportionment and sensitivity analysis: two methodologies with two different purposes, *Geoscientific Model Development*, 10, 4245–4256, <https://doi.org/10.5194/gmd-10-4245-2017>, 2017.
- Coates, J. and Butler, T. M.: A comparison of chemical mechanisms using tagged ozone production potential (TOPP) analysis, *Atmospheric Chemistry and Physics*, 15, 8795–8808, <https://doi.org/10.5194/acp-15-8795-2015>, 2015.
- Crutzen, P.: A discussion of the chemistry of some minor constituents in the stratosphere and troposphere, *Pure Appl. Geophys.*, 106, 1385–1399, 1973.
- Derwent, R. G.: Representing Organic Compound Oxidation in Chemical Mechanisms for Policy-Relevant Air Quality Models under Background Troposphere Conditions, *Atmosphere*, 11, 171, <https://doi.org/10.3390/atmos11020171>, 2020.
- Derwent, R. G., Utembe, S. R., Jenkin, M. E., and Shallcross, D. E.: Tropospheric ozone production regions and the intercontinental origins of surface ozone over Europe, *Atmospheric Environment*, 112, 216–224, <https://doi.org/10.1016/j.atmosenv.2015.04.049>, 2015.
- Derwent, R. G., Manning, A. J., Simmonds, P. G., Spain, T. G., and O'Doherty, S.: Long-term trends in ozone in baseline and European regionally-polluted air at Mace Head, Ireland over a 30-year period, *Atmospheric Environment*, 179, 279–287, <https://doi.org/10.1016/j.atmosenv.2018.02.024>, 2018.
- Dunker, A., Yarwood, G., Ortmann, J., and Wilson, G.: Comparison of source apportionment and source sensitivity of ozone in a three-dimensional air quality model, *Environmental Science and Technology*, 36, 2953–2964, <https://doi.org/10.1021/es011418f>, 2002.
- Emmerson, K. and Evans, M.: Comparison of tropospheric gas-phase chemistry schemes for use within global models, *Atmos. Chem. Phys.*, 9, 1831–1845, 2009.
- Emmons, L. K., Hess, P. G., Lamarque, J.-F., and Pfister, G. G.: Tagged ozone mechanism for MOZART-4, CAM-chem and other chemical transport models, *Geosci. Model Dev.*, 5, 1531–1542, <https://doi.org/10.5194/gmd-5-1531-2012>, <http://www.geosci-model-dev.net/5/1531/2012/>, 2012.



- Emmons, L. K., Arnold, S. R., Monks, S. A., Huijnen, V., Tilmes, S., Law, K. S., Thomas, J. L., Raut, J.-C., Bouarar, I., Turquety, S., Long, Y., Duncan, B., Steenrod, S., Strode, S., Flemming, J., Mao, J., Langner, J., Thompson, A. M., Tarasick, D., Apel, E. C., Blake, D. R.,
630 Cohen, R. C., Dibb, J., Diskin, G. S., Fried, A., Hall, S. R., Huey, L. G., Weinheimer, A. J., Wisthaler, A., Mikoviny, T., Nowak, J., Peischl, J., Roberts, J. M., Ryerson, T., Warneke, C., and Helmig, D.: The POLARCAT Model Intercomparison Project (POLMIP): overview and evaluation with observations, *Atmospheric Chemistry and Physics*, 15, 6721–6744, <https://doi.org/10.5194/acp-15-6721-2015>, 2015.
- Fiore, A. M., Fischer, E. V., Milly, G. P., Deolal, S. P., Wild, O., Jaffe, D. A., Staehelin, J., Clifton, O. E., Bergmann, D., Collins, W., Dentener, F., Doherty, R. M., Duncan, B. N., Fischer, B., Gilge, S., Hess, P. G., Horowitz, L. W., Lupu, A., MacKenzie, I. A., Park, R.,
635 Ries, L., Sanderson, M. G., Schultz, M. G., Shindell, D. T., Steinbacher, M., Stevenson, D. S., Szopa, S., Zellweger, C., and Zeng, G.: Peroxy acetyl nitrate (PAN) measurements at northern midlatitude mountain sites in April: a constraint on continental source–receptor relationships, *Atmospheric Chemistry and Physics*, 18, 15 345–15 361, <https://doi.org/10.5194/acp-18-15345-2018>, 2018.
- Fiore, A. M., West, J. J., Horowitz, L. W., Naik, V., and Schwarzkopf, M. D.: Characterizing the tropospheric ozone response to methane emission controls and the benefits to climate and air quality, *J. Geophys. Res.*, 113, D08 307, <https://doi.org/10.1029/2007JD009162>,
640 2008.
- Fiore, A. M., Dentener, F. J., Wild, O., Cuvelier, C., Schultz, M. G., Hess, P., Textor, C., Schulz, M., Doherty, R. M., Horowitz, L. W., MacKenzie, I. A., Sanderson, M. G., Shindell, D. T., Stevenson, D. S., Szopa, S., Van Dingenen, R., Zeng, G., Atherton, C., Bergmann, D., Bey, I., Carmichael, G., Collins, W. J., Duncan, B. N., Faluvegi, G., Folberth, G., Gauss, M., Gong, S., Hauglustaine, D., Holloway, T., Isak-
645 sen, I. S. A., Jacob, D. J., Jonson, J. E., Kaminski, J. W., Keating, T. J., Lupu, A., Marmer, E., Montanaro, V., Park, R. J., Pitari, G., Pringle, K. J., Pyle, J. A., Schroeder, S., Vivanco, M. G., Wind, P., Wojcik, G., Wu, S., and Zuber, A.: Multimodel estimates of intercontinental source-receptor relationships for ozone pollution, *J. Geophys. Res.*, 114, article number D04 301, <https://doi.org/10.1029/2008JD010816>, 2009.
- Fischer, E. V., Jacob, D. J., Yantosca, R. M., Sulprizio, M. P., Millet, D. B., Mao, J., Paulot, F., Singh, H. B., Roiger, A., Ries, L., Talbot, R., Dzepina, K., and Deolal, S. P.: Atmospheric peroxyacetyl nitrate (PAN): a global budget and source attribution, *Atmospheric Chemistry and Physics*, 14, 2679–2698, <https://doi.org/10.5194/acp-14-2679-2014>, 2014.
- Fleming, Z. L., Doherty, R. M., Schneidemesser, E. V., Malley, C. S., Cooper, O. R., Pinto, J. P., Colette, A., Xu, X., Simpson, D., Schultz, M. G., Lefohn, A. S., Hamad, S., Moolla, R., Solberg, S., and Feng, Z.: Tropospheric Ozone Assessment Report: Present-day ozone distribution and trends relevant to human health, *Elem Sci Anth*, 6, 12, <https://doi.org/10.1525/elementa.273>, 2018.
- Galloway, J. N., Townsend, A. R., Erisman, J. W., Bekunda, M., Cai, Z., Freney, J. R., Martinelli, L. A., Seitzinger, S. P., and
655 Sutton, M. A.: Transformation of the Nitrogen Cycle: Recent Trends, Questions, and Potential Solutions, *Science*, 320, 889–892, <https://doi.org/10.1126/science.1136674>, 2008.
- Galmarini, S., Koffi, B., Solazzo, E., Keating, T., Hogrefe, C., Schulz, M., Benedictow, A., Griesfeller, J. J., Janssens-Maenhout, G., Carmichael, G., Fu, J., and Dentener, F.: Technical note: Coordination and harmonization of the multi-scale, multi-model activities HTAP2, AQMEII3, and MICS-Asia3: simulations, emission inventories, boundary conditions, and model output formats, *Atmospheric Chemistry and Physics*, 17, 1543–1555, <https://doi.org/10.5194/acp-17-1543-2017>, <https://www.atmos-chem-phys.net/17/1543/2017/>, 2017.
- Goldstein, A. H. and Galbally, I. E.: Known and unexplored organic constituents in the earth’s atmosphere, *Environ. Sci. Technol.*, 41, 1514–1521, 2007.
- Grewe, V., Tsati, E., and Hoor, P.: On the attribution of contributions of atmospheric trace gases to emissions in atmospheric model applications, *Geoscientific Model Development*, 3, 487–499, <https://doi.org/10.5194/gmd-3-487-2010>, 2010.



- 665 Grewe, V., Tsati, E., Mertens, M., Frömming, C., and Jöckel, P.: Contribution of emis-
sions to concentrations: the TAGGING 1.0 submodel based on the Modular Earth Submodel
System (MESSy 2.52), *Geoscientific Model Development*, 10, 2615–2633, <https://doi.org/10.5194/gmd-10-2615-2017>,
<https://www.geosci-model-dev.net/10/2615/2017/>, 2017.
- Han, H., Liu, J., Yuan, H., Wang, T., Zhuang, B., and Zhang, X.: Foreign influences on tropospheric ozone over East Asia through global
670 atmospheric transport, *Atmospheric Chemistry and Physics*, 19, 12495–12514, <https://doi.org/10.5194/acp-19-12495-2019>, 2019.
- Heald, C. L. and Kroll, J. H.: The fuel of atmospheric chemistry: Toward a complete description of reactive organic carbon, *Science Advances*,
6, eaay8967, <https://doi.org/10.1126/sciadv.aay8967>, 2020.
- Hoor, P., Borken-Kleefeld, J., Caro, D., Dessens, O., Endresen, O., Gauss, M., Grewe, V., Hauglustaine, D., Isaksen, I. S. A., Jöckel, P.,
Lelieveld, J., Myhre, G., Meijer, E., Olivie, D., Prather, M., Poberaj, C. S., Shine, K. P., Staehelin, J., Tang, Q., van Aardenne, J., van
675 Velthoven, P., and Sausen, R.: The impact of traffic emissions on atmospheric ozone and OH: results from QUANTIFY, *Atmospheric
Chemistry and Physics*, 9, 3113–3136, <https://doi.org/10.5194/acp-9-3113-2009>, 2009.
- HTAP: Hemispheric Transport of Air Pollution 2010, Part A: Ozone and Particulate Matter, United Nations Publication ECE/EB.AIR/100,
edited by: Dentener, F., Keating, T., Akimoto, H., 2010.
- Huang, M., Carmichael, G. R., Pierce, R. B., Jo, D. S., Park, R. J., Flemming, J., Emmons, L. K., Bowman, K. W., Henze, D. K., Davila, Y.,
680 Sudo, K., Jonson, J. E., Tronstad Lund, M., Janssens-Maenhout, G., Dentener, F. J., Keating, T. J., Oetjen, H., and Payne, V. H.: Impact of
intercontinental pollution transport on North American ozone air pollution: an HTAP phase 2 multi-model study, *Atmospheric Chemistry
and Physics*, 17, 5721–5750, <https://doi.org/10.5194/acp-17-5721-2017>, <https://www.atmos-chem-phys.net/17/5721/2017/>, 2017.
- Jacob, D., Heikes, B., Fan, S., Logan, J., Mauzerall, D., Bradshaw, J., Singh, H., Gregory, G., Talbot, R., Blake, D., and Sachse, G.: Origin
of ozone and NO_x in the tropical troposphere: A photochemical analysis of aircraft observations over the South Atlantic basin, *Journal of*
685 *Geophysical Research: Oceans*, 101, 24235–24250, 1996.
- Jacob, D., Logan, J., and Murti, P.: Effect of rising Asian emissions on surface ozone in the United States, *Geophys. Res. Lett.*, 26, 2175–
2178, <https://doi.org/10.1029/1999GL900450>, 1999.
- Janssens-Maenhout, G., Crippa, M., Guizzardi, D., Dentener, F., Muntean, M., Pouliot, G., Keating, T., Zhang, Q., Kurokawa, J., Wankmüller,
R., Denier van der Gon, H., Kuenen, J. J. P., Klimont, Z., Frost, G., Darras, S., Koffi, B., and Li, M.: HTAP_v2.2: a mosaic of regional
690 and global emission grid maps for 2008 and 2010 to study hemispheric transport of air pollution, *Atmospheric Chemistry and Physics*, 15,
11411–11432, <https://doi.org/10.5194/acp-15-11411-2015>, <https://www.atmos-chem-phys.net/15/11411/2015/>, 2015.
- Jonson, J. E., Schulz, M., Emmons, L., Flemming, J., Henze, D., Sudo, K., Lund, M. T., Lin, M., Benedictow, A., Koffi, B., Dentener,
F., Keating, T., Kivi, R., and Davila, Y.: The effects of intercontinental emission sources on European air pollution levels, *Atmospheric
Chemistry and Physics*, 18, 13655–13672, <https://doi.org/10.5194/acp-18-13655-2018>, 2018.
- 695 Jonson, J. E., Gauss, M., Schulz, M., Jalkanen, J.-P., and Fagerli, H.: Effects of global ship emissions on European air pollution levels,
Atmospheric Chemistry and Physics Discussions, <https://doi.org/10.5194/acp-2020-293>, 2020.
- Kasibhatla, P., Levy, H., Moxim, W. J., Pandis, S. N., Corbett, J. J., Peterson, M. C., Honrath, R. E., Frost, G. J., Knapp, K., Parrish, D. D.,
and Ryerson, T. B.: Do emissions from ships have a significant impact on concentrations of nitrogen oxides in the marine boundary layer?,
Geophysical Research Letters, 27, 2229–2232, <https://doi.org/10.1029/2000gl011387>, 2000.
- 700 Kleinman, L. I., Daum, P. H., Imre, D., Lee, Y.-N., Nunnermacker, L. J., Springston, S. R., Weinstein-Lloyd, J., and Rudolph, J.: Ozone
production rate and hydrocarbon reactivity in 5 urban areas: A cause of high ozone concentration in Houston, *Geophysical Research
Letters*, 29, 105–1–105–4, <https://doi.org/10.1029/2001gl014569>, 2002.



- 705 Knote, C., Tuccella, P., Curci, G., Emmons, L., Orlando, J. J., Madronich, S., Baró, R., Jiménez-Guerrero, P., Luecken, D., Hogrefe, C., Forkel, R., Werhahn, J., Hirtl, M., Pérez, J. L., José, R. S., Giordano, L., Brunner, D., Yahya, K., and Zhang, Y.: Influence of the choice of gas-phase mechanism on predictions of key gaseous pollutants during the AQMEII phase-2 intercomparison, *Atmospheric Environment*, 115, 553–568, <https://doi.org/10.1016/j.atmosenv.2014.11.066>, 2015.
- 710 Lamarque, J.-F., Emmons, L. K., Hess, P. G., Kinnison, D. E., Tilmes, S., Vitt, F., Heald, C. L., Holland, E. A., Lauritzen, P. H., Neu, J., Orlando, J. J., Rasch, P. J., and Tyndall, G. K.: CAM-chem: description and evaluation of interactive atmospheric chemistry in the Community Earth System Model, *Geoscientific Model Development*, 5, 369–411, <https://doi.org/10.5194/gmd-5-369-2012>, <https://www.geosci-model-dev.net/5/369/2012/>, 2012.
- Lawrence, M. G. and Crutzen, P. J.: Influence of NO_x emissions from ships on tropospheric photochemistry and climate, *Nature*, 402, 167–170, <https://doi.org/10.1038/46013>, 1999.
- Li, K., Jacob, D. J., Liao, H., Shen, L., Zhang, Q., and Bates, K. H.: Anthropogenic drivers of 2013–2017 trends in summer surface ozone in China, *Proceedings of the National Academy of Sciences*, 116, 422–427, <https://doi.org/10.1073/pnas.1812168116>, 2018.
- 715 Li, M., Zhang, Q., Zheng, B., Tong, D., Lei, Y., Liu, F., Hong, C., Kang, S., Yan, L., Zhang, Y., Bo, Y., Su, H., Cheng, Y., and He, K.: Persistent growth of anthropogenic non-methane volatile organic compound (NMVOC) emissions in China during 1990–2017: drivers, speciation and ozone formation potential, *Atmospheric Chemistry and Physics*, 19, 8897–8913, <https://doi.org/10.5194/acp-19-8897-2019>, 2019.
- Lin, M., Fiore, A. M., Horowitz, L. W., Cooper, O. R., Naik, V., Holloway, J., Johnson, B. J., Middlebrook, A. M., Oltmans, S. J., Pollack, I. B., Ryerson, T. B., Warner, J. X., Wiedinmyer, C., Wilson, J., and Wyman, B.: Transport of Asian ozone pollution into surface air over the western United States in spring, *Journal of Geophysical Research: Atmospheres*, 117, n/a–n/a, <https://doi.org/10.1029/2011jd016961>, 2012.
- 720 Liu, F., Beirle, S., Zhang, Q., van der A, R. J., Zheng, B., Tong, D., and He, K.: NO_x emission trends over Chinese cities estimated from OMI observations during 2005 to 2015, *Atmospheric Chemistry and Physics*, 17, 9261–9275, <https://doi.org/10.5194/acp-17-9261-2017>, 2017.
- 725 Lupaşcu, A. and Butler, T.: Source attribution of European surface O₃ using a tagged O₃ mechanism, *Atmospheric Chemistry and Physics*, 19, 14 535–14 558, <https://doi.org/10.5194/acp-19-14535-2019>, 2019.
- Mertens, M., Grewe, V., Rieger, V. S., and Jöckel, P.: Revisiting the contribution of land transport and shipping emissions to tropospheric ozone, *Atmospheric Chemistry and Physics*, 18, 5567–5588, <https://doi.org/10.5194/acp-18-5567-2018>, 2018.
- 730 Mills, G., Pleijel, H., Malley, C. S., Sinha, B., Cooper, O. R., Schultz, M. G., Neufeld, H. S., Simpson, D., Sharps, K., Feng, Z., Gerosa, G., Harmens, H., Kobayashi, K., Saxena, P., Paoletti, E., Sinha, V., and Xu, X.: Tropospheric Ozone Assessment Report: Present-day tropospheric ozone distribution and trends relevant to vegetation, *Elem Sci Anth*, 6, 47, <https://doi.org/10.1525/elementa.302>, 2018.
- Monks, P., Archibald, A., Colette, A., Cooper, O., Coyle, M., Derwent, R., Fowler, D., Granier, C., Law, K., Mills, G., Stevenson, D., Tarasova, O., Thouret, V., Von Schneidmesser, E., Sommariva, R., Wild, O., and Williams, M.: Tropospheric ozone and its precursors from the urban to the global scale from air quality to short-lived climate forcer, *Atmospheric Chemistry and Physics*, 15, 8889–8973, <https://doi.org/10.5194/acp-15-8889-2015>, 2015.
- 735 Myhre, G., Shine, K., Rädcl, G., Gauss, M., Isaksen, I., Tang, Q., Prather, M., Williams, J., van Velthoven, P., Dessens, O., Koffi, B., Szopa, S., Hoor, P., Grewe, V., Borken-Kleefeld, J., Berntsen, T., and Fuglestedt, J.: Radiative forcing due to changes in ozone and methane caused by the transport sector, *Atmospheric Environment*, 45, 387–394, <https://doi.org/10.1016/j.atmosenv.2010.10.001>, 2011.
- 740 Ni, R., Lin, J., Yan, Y., and Lin, W.: Foreign and domestic contributions to springtime ozone over China, *Atmospheric Chemistry and Physics*, 18, 11 447–11 469, <https://doi.org/10.5194/acp-18-11447-2018>, 2018.



- Parrish, D. D., Petropavlovskikh, I., and Oltmans, S. J.: Reversal of Long-Term Trend in Baseline Ozone Concentrations at the North American West Coast, *Geophysical Research Letters*, 44, 10,675–10,681, <https://doi.org/10.1002/2017gl074960>, 2017.
- Prather, M. J.: Time scales in atmospheric chemistry: Theory, GWPs for CH₄ and CO, and runaway growth, *Geophys. Res. Lett.*, 23, 2597–2600, 1996.
- 745 Rao, S., Klimont, Z., Smith, S. J., Dingenen, R. V., Dentener, F., Bouwman, L., Riahi, K., Amann, M., Bodirsky, B. L., van Vuuren, D. P., Reis, L. A., Calvin, K., Drouet, L., Fricko, O., Fujimori, S., Gernaat, D., Havlik, P., Harmsen, M., Hasegawa, T., Heyes, C., Hilaire, J., Luderer, G., Masui, T., Stehfest, E., Strefler, J., van der Sluis, S., and Tavoni, M.: Future air pollution in the Shared Socio-economic Pathways, *Global Environmental Change*, 42, 346–358, <https://doi.org/10.1016/j.gloenvcha.2016.05.012>, 2017.
- Reidmiller, D. R., Fiore, A. M., Jaffe, D. A., Bergmann, D., Cuvelier, C., Dentener, F. J., Duncan, B. N., Folberth, G., Gauss, M., Gong, S., 750 Hess, P., Jonson, J. E., Keating, T., Lupu, A., Marmer, E., Park, R., Schultz, M. G., Shindell, D. T., Szopa, S., Vivanco, M. G., Wild, O., and Zuber, A.: The influence of foreign vs. North American emissions on surface ozone in the US, *Atmospheric Chemistry and Physics*, 9, 5027–5042, <https://doi.org/10.5194/acp-9-5027-2009>, 2009.
- Rienecker, M. M., Suarez, M. J., Gelaro, R., Todling, R., Bacmeister, J., Liu, E., Bosilovich, M. G., Schubert, S. D., Takacs, L., Kim, G.-K., Bloom, S., Chen, J., Collins, D., Conaty, A., da Silva, A., Gu, W., Joiner, J., Koster, R. D., Lucchesi, R., Molod, A., Owens, T., Pawson, 755 S., Pegion, P., Redder, C. R., Reichle, R., Robertson, F. R., Ruddick, A. G., Sienkiewicz, M., and Woollen, J.: MERRA: NASA's Modern-Era Retrospective Analysis for Research and Applications, *Journal of Climate*, 24, 3624–3648, <https://doi.org/10.1175/jcli-d-11-00015.1>, 2011.
- Saunders, S. M., Jenkin, M. E., Derwent, R. G., and Pilling, M. J.: Protocol for the development of the Master Chemical Mechanism, MCM v3 (Part A): tropospheric degradation of non-aromatic volatile organic compounds, *Atmos. Chem. Phys.*, 3, 161–180, 2003.
- 760 Saunio, M., Bousquet, P., Poulter, B., Peregón, A., Ciais, P., Canadell, J. G., Dlugokencky, E. J., Etiope, G., Bastviken, D., Houweling, S., Janssens-Maenhout, G., Tubiello, F. N., Castaldi, S., Jackson, R. B., Alexe, M., Arora, V. K., Beerling, D. J., Bergamaschi, P., Blake, D. R., Brailsford, G., Brovkin, V., Bruhwiler, L., Crevoisier, C., Crill, P., Covey, K., Curry, C., Frankenberg, C., Gedney, N., Höglund-Isaksson, L., Ishizawa, M., Ito, A., Joos, F., Kim, H.-S., Kleinen, T., Krummel, P., Lamarque, J.-F., Langenfelds, R., Locatelli, R., Machida, T., Maksyutov, S., McDonald, K. C., Marshall, J., Melton, J. R., Morino, I., Naik, V., ODoherty, S., Parmentier, F.-J. W., Patra, P. K., Peng, 765 C., Peng, S., Peters, G. P., Pison, I., Prigent, C., Prinn, R., Ramonet, M., Riley, W. J., Saito, M., Santini, M., Schroeder, R., Simpson, I. J., Spahni, R., Steele, P., Takizawa, A., Thornton, B. F., Tian, H., Tohjima, Y., Viovy, N., Voulgarakis, A., van Weele, M., van der Werf, G. R., Weiss, R., Wiedinmyer, C., Wilton, D. J., Wiltshire, A., Worthy, D., Wunch, D., Xu, X., Yoshida, Y., Zhang, B., Zhang, Z., and Zhu, Q.: The global methane budget 2000–2012, *Earth System Science Data*, 8, 697–751, <https://doi.org/10.5194/essd-8-697-2016>, 2016.
- Schultz, M. G., Schröder, S., Lyapina, O., Cooper, O., Galbally, I., Petropavlovskikh, I., Schneidemesser, E. V., Tanimoto, H., Elshorbany, 770 Y., Naja, M., Seguel, R., Dauert, U., Eckhardt, P., Feigenspahn, S., Fiebig, M., Hjellbrekke, A.-G., Hong, Y.-D., Kjeld, P. C., Koide, H., Lear, G., Tarasick, D., Ueno, M., Wallasch, M., Baumgardner, D., Chuang, M.-T., Gillett, R., Lee, M., Molloy, S., Moolla, R., Wang, T., Sharps, K., Adame, J. A., Ancellet, G., Apadula, F., Artaxo, P., Barlasina, M., Bogucka, M., Bonasoni, P., Chang, L., Colomb, A., Cuevas, E., Cupeiro, M., Degorska, A., Ding, A., Fröhlich, M., Frolova, M., Gadhavi, H., Gheusi, F., Gilge, S., Gonzalez, M. Y., Gros, V., Hamad, S. H., Helmig, D., Henriques, D., Hermansen, O., Holla, R., Huber, J., Im, U., Jaffe, D. A., Komala, N., Kubistin, D., Lam, K.-S., Laurila, 775 T., Lee, H., Levy, I., Mazzoleni, C., Mazzoleni, L., McClure-Begley, A., Mohamad, M., Murovic, M., Navarro-Comas, M., Nicodim, F., Parrish, D., Read, K. A., Reid, N., Ries, L., Saxena, P., Schwab, J. J., Scorgie, Y., Senik, I., Simmonds, P., Sinha, V., Skorokhod, A., Spain, G., Spangl, W., Spoor, R., Springston, S. R., Steer, K., Steinbacher, M., Suharguniyawan, E., Torre, P., Trickl, T., Weili, L., Weller,



- R., Xu, X., Xue, L., and Zhiqiang, M.: Tropospheric Ozone Assessment Report: Database and Metrics Data of Global Surface Ozone Observations, *Elem Sci Anth*, 5, 58, <https://doi.org/10.1525/elementa.244>, 2017.
- 780 Stevenson, D., Young, P., Naik, V., Lamarque, J.-F., Shindell, D., Voulgarakis, A., Skeie, R., Dalsoren, S., Myhre, G., Berntsen, T., Folberth, G., Rumbold, S., Collins, W., MacKenzie, I., Doherty, R., Zeng, G., Van Noije, T., Strunk, A., Bergmann, D., Cameron-Smith, P., Plummer, D., Strode, S., Horowitz, L., Lee, Y., Szopa, S., Sudo, K., Nagashima, T., Josse, B., Cionni, I., Righi, M., Eyring, V., Conley, A., Bowman, K., Wild, O., and Archibald, A.: Tropospheric ozone changes, radiative forcing and attribution to emissions in the Atmospheric Chemistry and Climate Model Intercomparison Project (ACCMIP), *Atmos. Chem. Phys.*, 13, 3063–3085, 2013.
- 785 Thunis, P., Clappier, A., Tarrason, L., Cuvelier, C., Monteiro, A., Pisoni, E., Wesseling, J., Belis, C., Pirovano, G., Janssen, S., Guerreiro, C., and Peduzzi, E.: Source apportionment to support air quality planning: Strengths and weaknesses of existing approaches, *Environment International*, 130, 104 825, <https://doi.org/10.1016/j.envint.2019.05.019>, 2019.
- Tilmes, S., Lamarque, J.-F., Emmons, L. K., Kinnison, D. E., Ma, P.-L., Liu, X., Ghan, S., Bardeen, C., Arnold, S., Deeter, M., Vitt, F., Ryerson, T., Elkins, J. W., Moore, F., Spackman, J. R., and Martin, M. V.: Description and evaluation of tropospheric chemistry and aerosols in the Community Earth System Model (CESM1.2), *Geoscientific Model Development*, 8, 1395–1426, <https://doi.org/10.5194/gmd-8-1395-2015>, 2015.
- Turner, A. J., Frankenberg, C., and Kort, E. A.: Interpreting contemporary trends in atmospheric methane, *Proceedings of the National Academy of Sciences*, 116, 2805–2813, <https://doi.org/10.1073/pnas.1814297116>, 2019.
- Utembe, S., Cooke, M., Archibald, A., Jenkin, M., Derwent, R., and Shallcross, D.: Using a reduced Common Representative Intermediates (CRIv2-R5) mechanism to simulate tropospheric ozone in a 3-D Lagrangian chemistry transport model, *Atmos. Environ.*, 44, 1609–1622, 2010.
- van der Werf, G. R., Randerson, J. T., Giglio, L., Collatz, G. J., Mu, M., Kasibhatla, P. S., Morton, D. C., DeFries, R. S., Jin, Y., and van Leeuwen, T. T.: Global fire emissions and the contribution of deforestation, savanna, forest, agricultural, and peat fires (1997–2009), *Atmospheric Chemistry and Physics*, 10, 11 707–11 735, <https://doi.org/10.5194/acp-10-11707-2010>, 2010.
- 800 Vinken, G. C. M., Boersma, K. F., Jacob, D. J., and Meijer, E. W.: Accounting for non-linear chemistry of ship plumes in the GEOS-Chem global chemistry transport model, *Atmospheric Chemistry and Physics*, 11, 11 707–11 722, <https://doi.org/10.5194/acp-11-11707-2011>, 2011.
- von Glasow, R., Lawrence, M. G., Sander, R., and Crutzen, P. J.: Modeling the chemical effects of ship exhaust in the cloud-free marine boundary layer, *Atmospheric Chemistry and Physics*, 3, 233–250, <https://doi.org/10.5194/acp-3-233-2003>, 2003.
- 805 Wang, Y. and Jacob, D. J.: Anthropogenic forcing on tropospheric ozone and OH since preindustrial times, *Journal of Geophysical Research: Atmospheres*, 103, 31 123–31 135, <https://doi.org/10.1029/1998jd100004>, 1998.
- Wang, Y., Jacob, D. J., and Logan, J. A.: Global simulation of tropospheric O₃-NO_x-hydrocarbon chemistry: 3. Origin of tropospheric ozone and effects of nonmethane hydrocarbons, *Journal of Geophysical Research: Atmospheres*, 103, 10 757–10 767, <https://doi.org/10.1029/98jd00156>, 1998.
- 810 Young, P., Archibald, A., Bowman, K., Lamarque, J.-F., Naik, V., Stevenson, D., Tilmes, S., Voulgarakis, A., Wild, O., Bergmann, D., Cameron-Smith, P., Cionni, I., Collins, W., Dalsoren, S., Doherty, R., Eyring, V., Faluvegi, G., Horowitz, L., Josse, B., Lee, Y., MacKenzie, I., Nagashima, T., Plummer, D., Righi, M., Rumbold, S., Skeie, R., Shindell, D., Strode, S., Sudo, K., Szopa, S., and Zeng, G.: Pre-industrial to end 21st century projections of tropospheric ozone from the atmospheric chemistry and climate model intercomparison project (ACCMIP), *Atmos. Chem. Phys.*, 13, 5401–5402, 2013.



- 815 Young, P. J., Naik, V., Fiore, A. M., Gaudel, A., Guo, J., Lin, M. Y., Neu, J. L., Parrish, D. D., Rieder, H. E., Schnell, J. L., Tilmes, S., Wild, O., Zhang, L., Ziemke, J. R., Brandt, J., Delcloo, A., Doherty, R. M., Geels, C., Hegglin, M. I., Hu, L., Im, U., Kumar, R., Luhar, A., Murray, L., Plummer, D., Rodriguez, J., Saiz-Lopez, A., Schultz, M. G., Woodhouse, M. T., and Zeng, G.: Tropospheric Ozone Assessment Report: Assessment of global-scale model performance for global and regional ozone distributions, variability, and trends, *Elem Sci Anth*, 6, 10, <https://doi.org/10.1525/elementa.265>, 2018.
- 820 Zhang, Y., Cooper, O. R., Gaudel, A., Thompson, A. M., Nédélec, P., Ogino, S.-Y., and West, J. J.: Tropospheric ozone change from 1980 to 2010 dominated by equatorward redistribution of emissions, *Nature Geoscience*, 9, 875–879, <https://doi.org/10.1038/ngeo2827>, 2016.

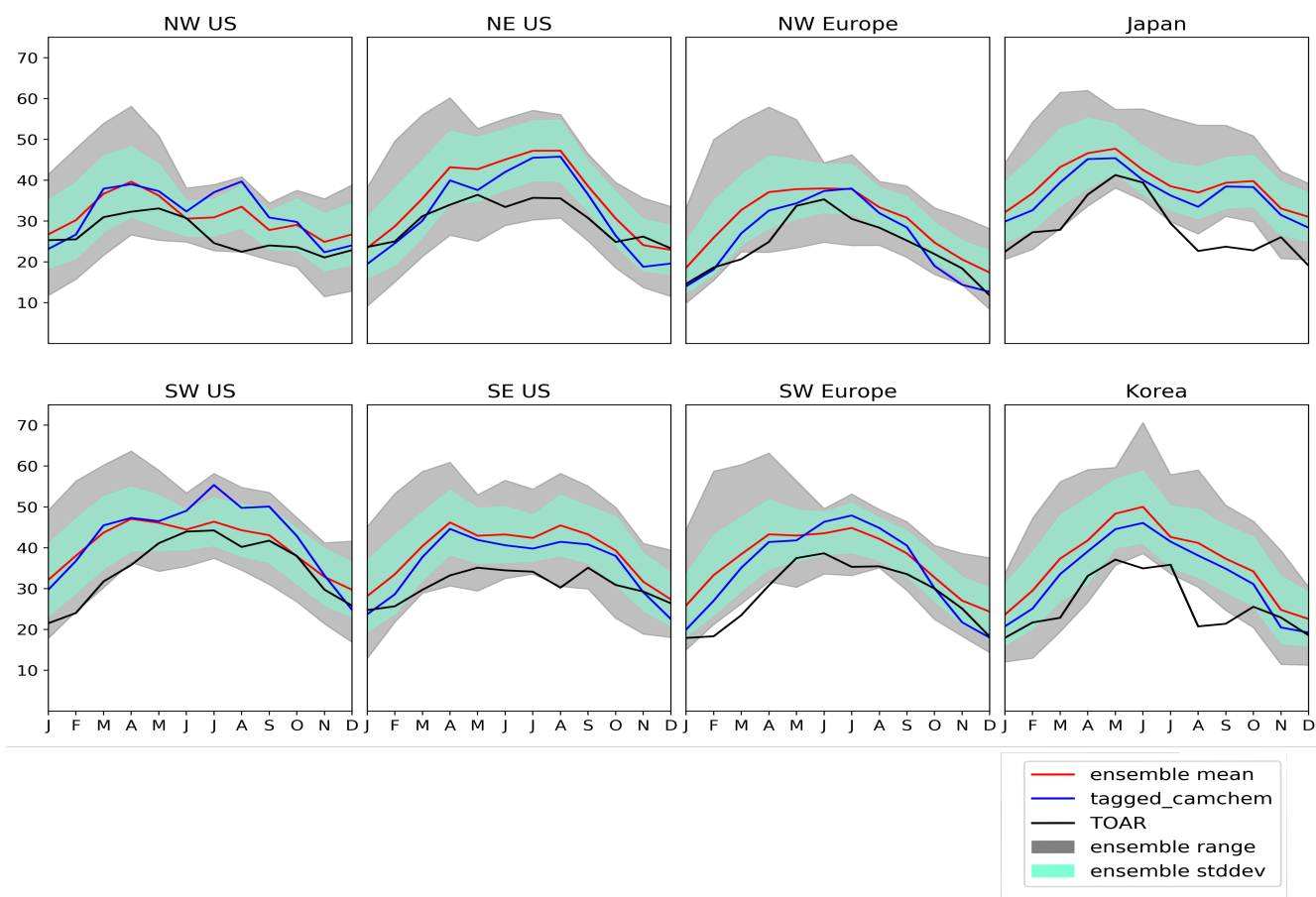


Figure 1. Seasonal cycle of monthly mean surface ozone (ppb) in HTAP Tier 2 regions from our base model run (blue line), compared with with observations from TOAR (black line), and other models from the HTAP ensemble of global models: ensemble mean (red line); ensemble standard deviation (green shaded area); and ensemble range (grey shaded area). Only grid cells containing TOAR observations have been used.

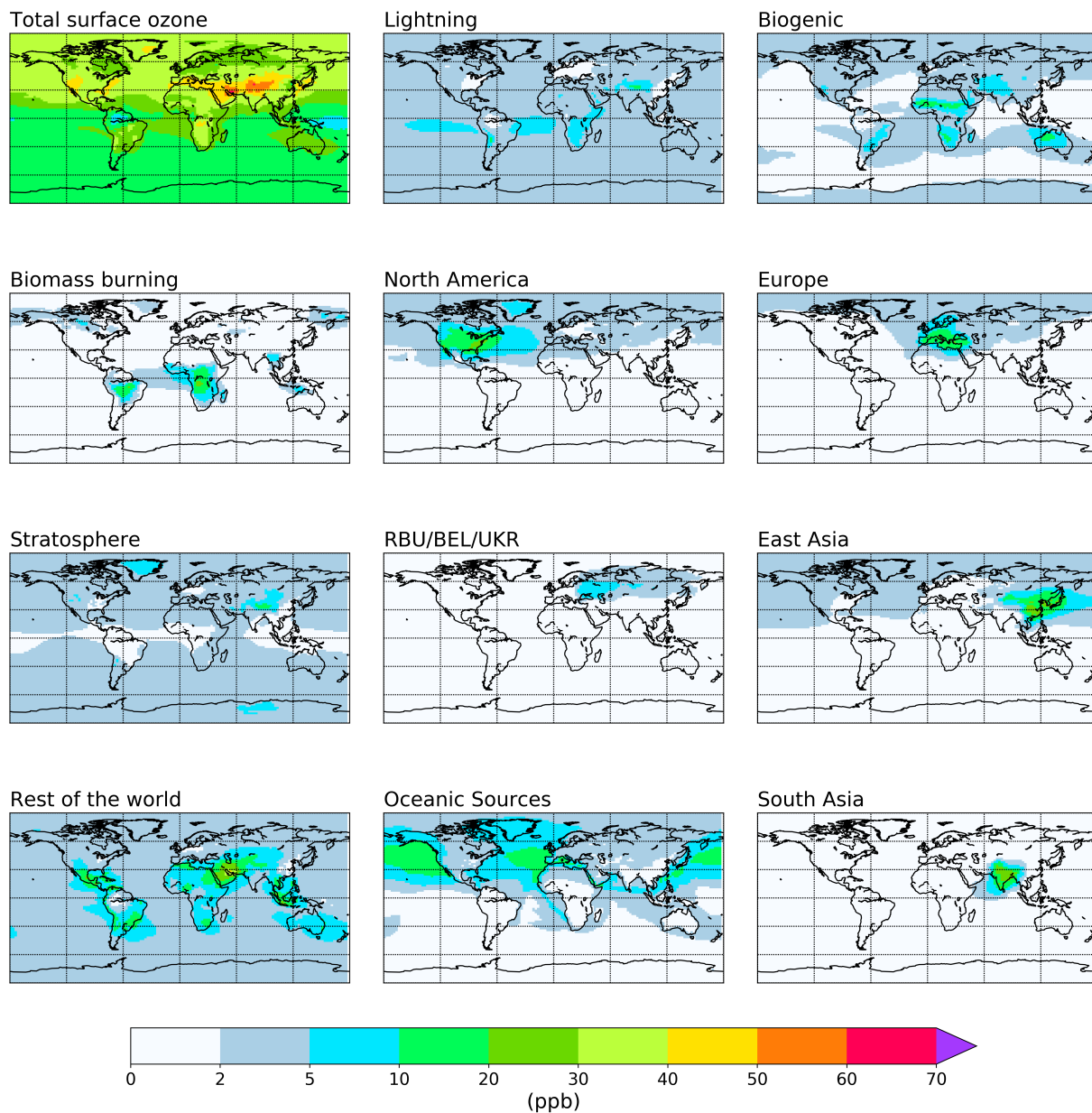


Figure 2. Annual mean surface ozone (ppb) from the NO_x -tagged base run. Total ozone is shown in the top left panel. Tagged ozone tracers are shown in other panels.

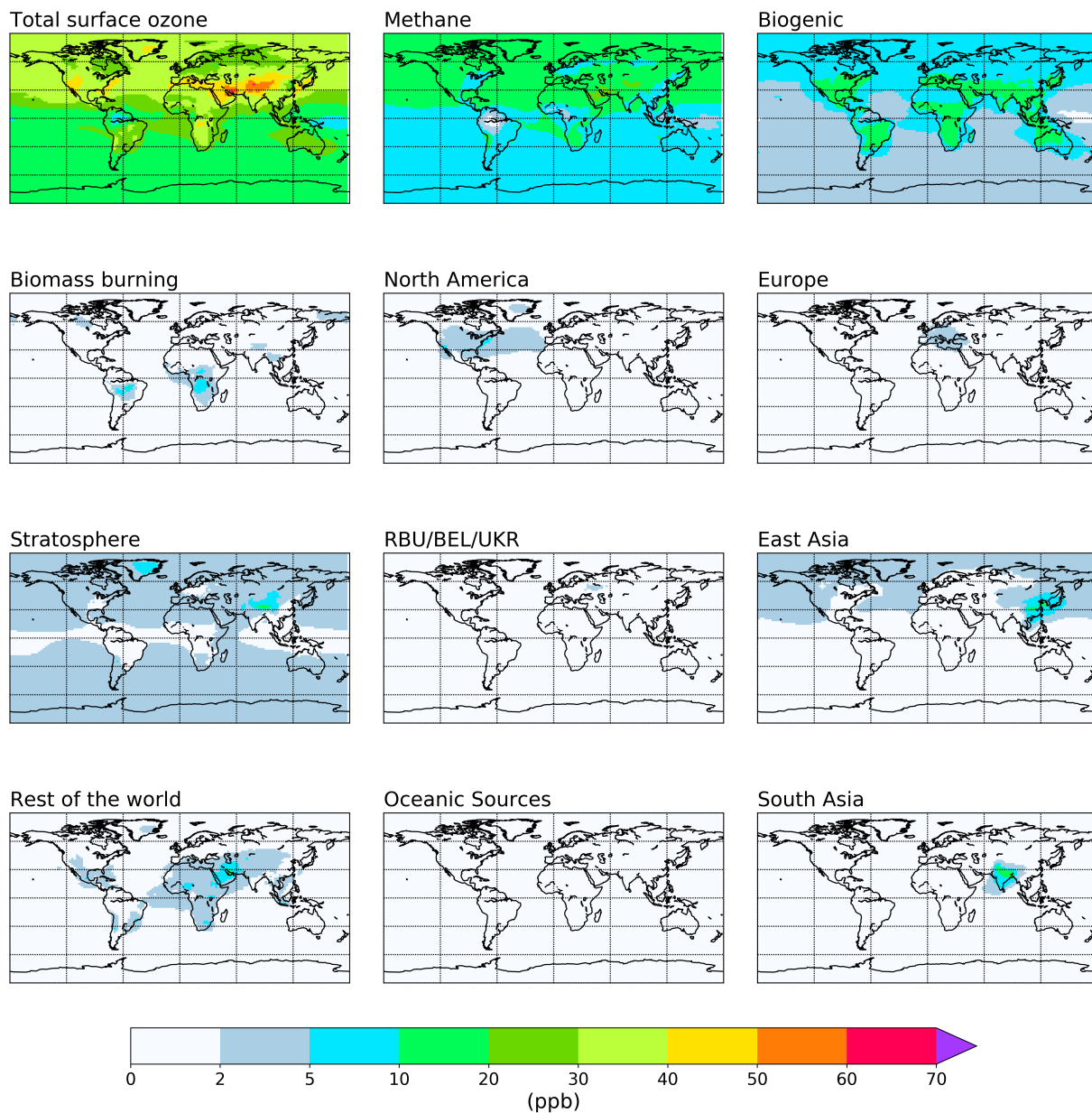


Figure 3. Annual mean surface ozone (ppb) from the VOC-tagged base run. Total ozone is shown in the top left panel. Tagged ozone tracers are shown in other panels.

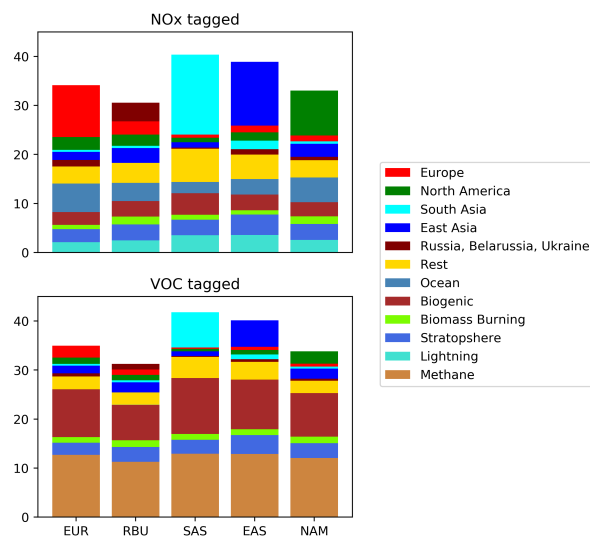


Figure 4. Source-receptor relationships for major Northern Hemisphere Tier 1 regions EUR (Europe); RBU (Russia, Belarus, and Ukraine); SAS (South Asia); EAS (East Asia); and NAM (North America). Annual average ozone (ppb) is shown for each region with attribution to NO_x emissions (top panel) and reactive carbon emissions (bottom panel) from all other HTAP Tier 1 regions.

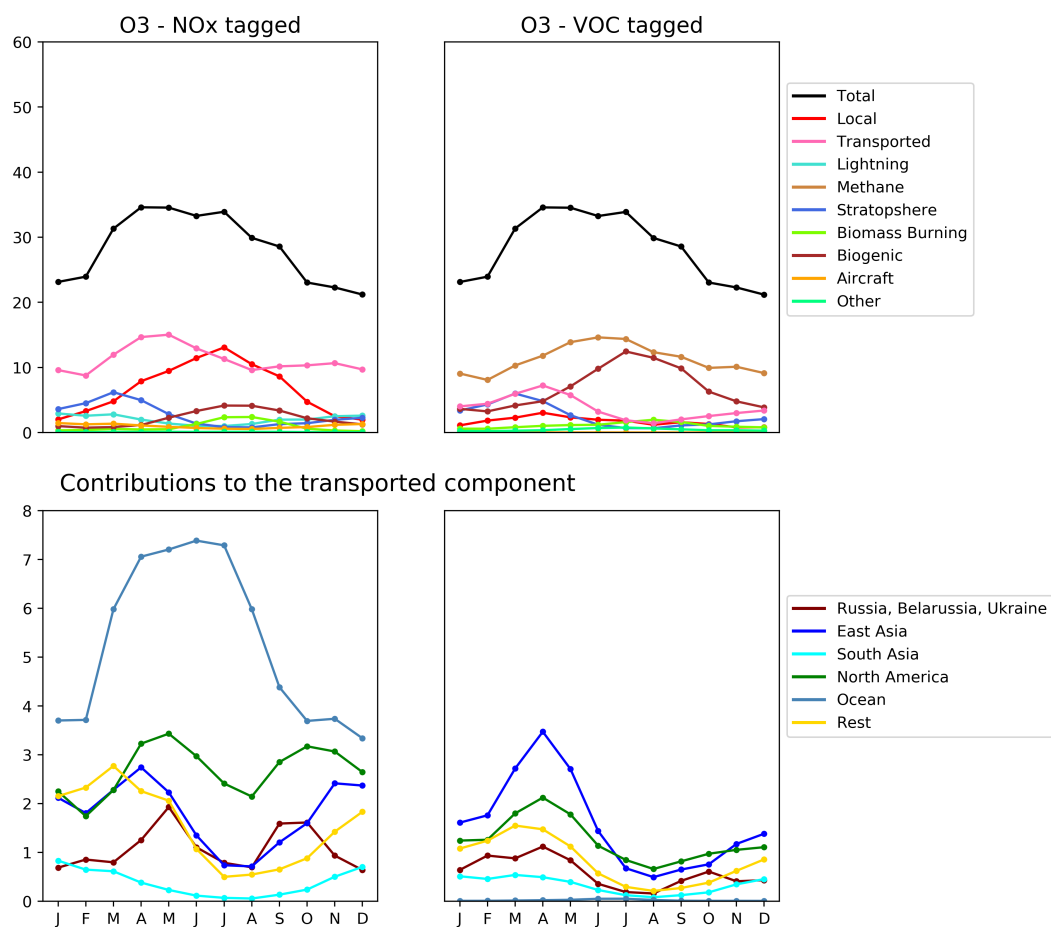


Figure 5. Seasonal cycle of surface ozone (ppb) in the HTAP Tier 2 receptor region “North West Europe”. NO_x -tagging is shown in the left panels, and reactive carbon tagging in the right panels. Top panels show total monthly mean ozone (black line) as well as the local anthropogenic component, long-range transported anthropogenic component, and natural components. Bottom panels show the individual Tier 1 source regions responsible for the long-range transported component of ozone.

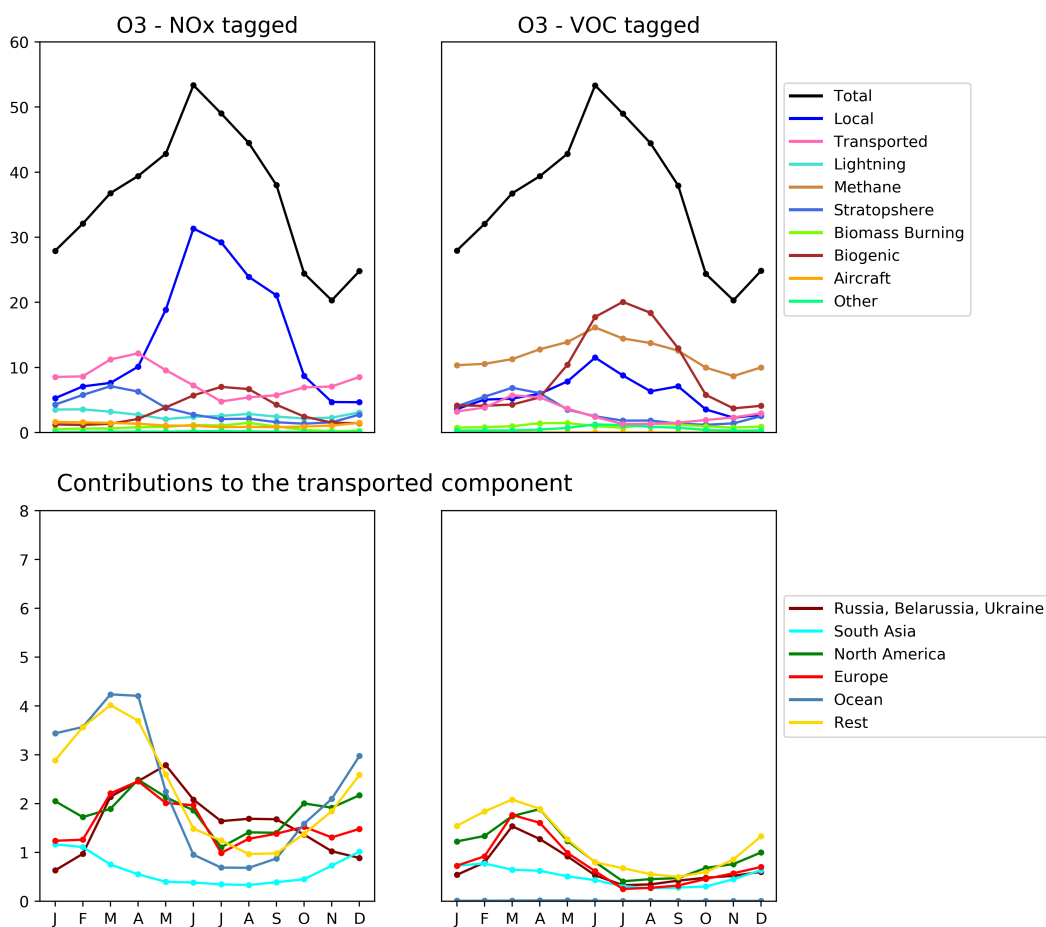


Figure 6. Seasonal cycle of surface ozone (ppb) in the HTAP Tier 2 receptor region “North East China”. NO_x-tagging is shown in the left panels, and reactive carbon tagging in the right panels. Top panels show total monthly mean ozone (black line) as well as the local anthropogenic component, long-range transported anthropogenic component, and natural components. Bottom panels show the individual Tier 1 source regions responsible for the long-range transported component of ozone.

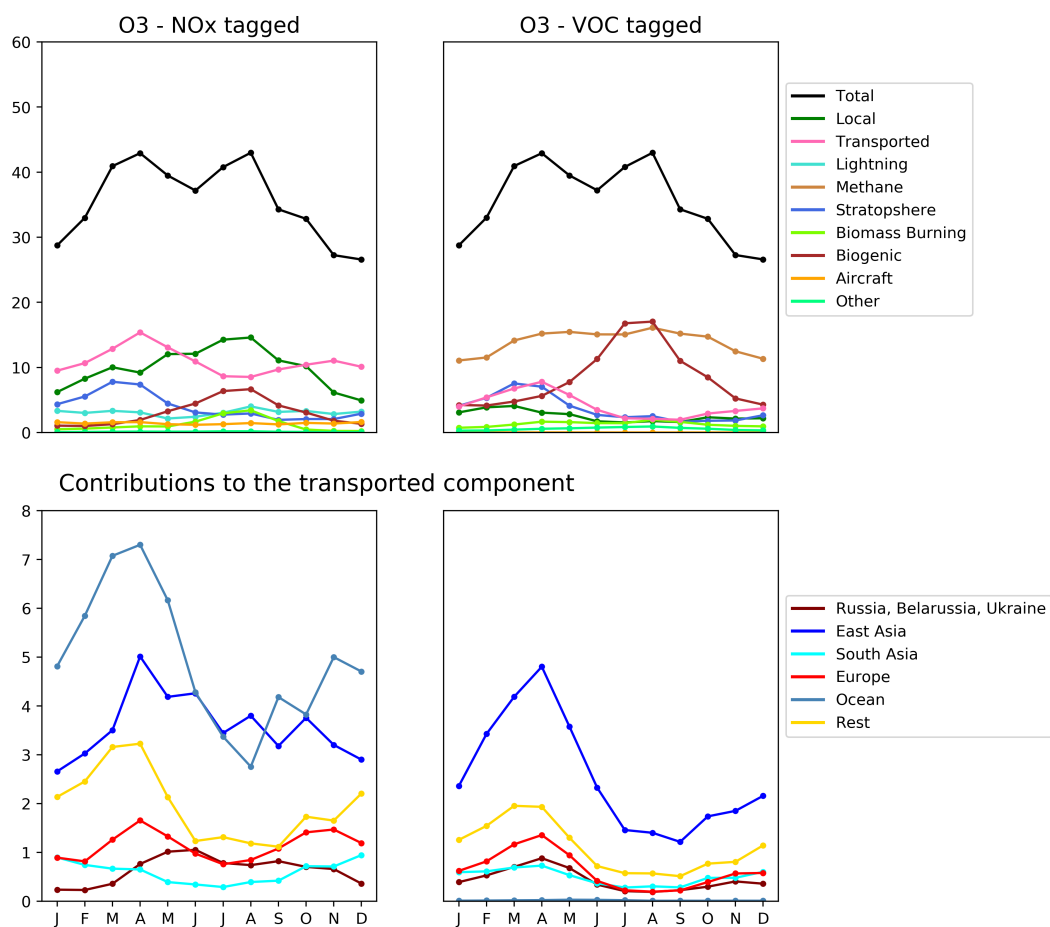


Figure 7. Seasonal cycle of surface ozone (ppb) in the HTAP Tier 2 receptor region “North West United States”. NO_x-tagging is shown in the left panels, and reactive carbon tagging in the right panels. Top panels show total monthly mean ozone (black line) as well as the local anthropogenic component, long-range transported anthropogenic component, and natural components. Bottom panels show the individual Tier 1 source regions responsible for the long-range transported component of ozone.

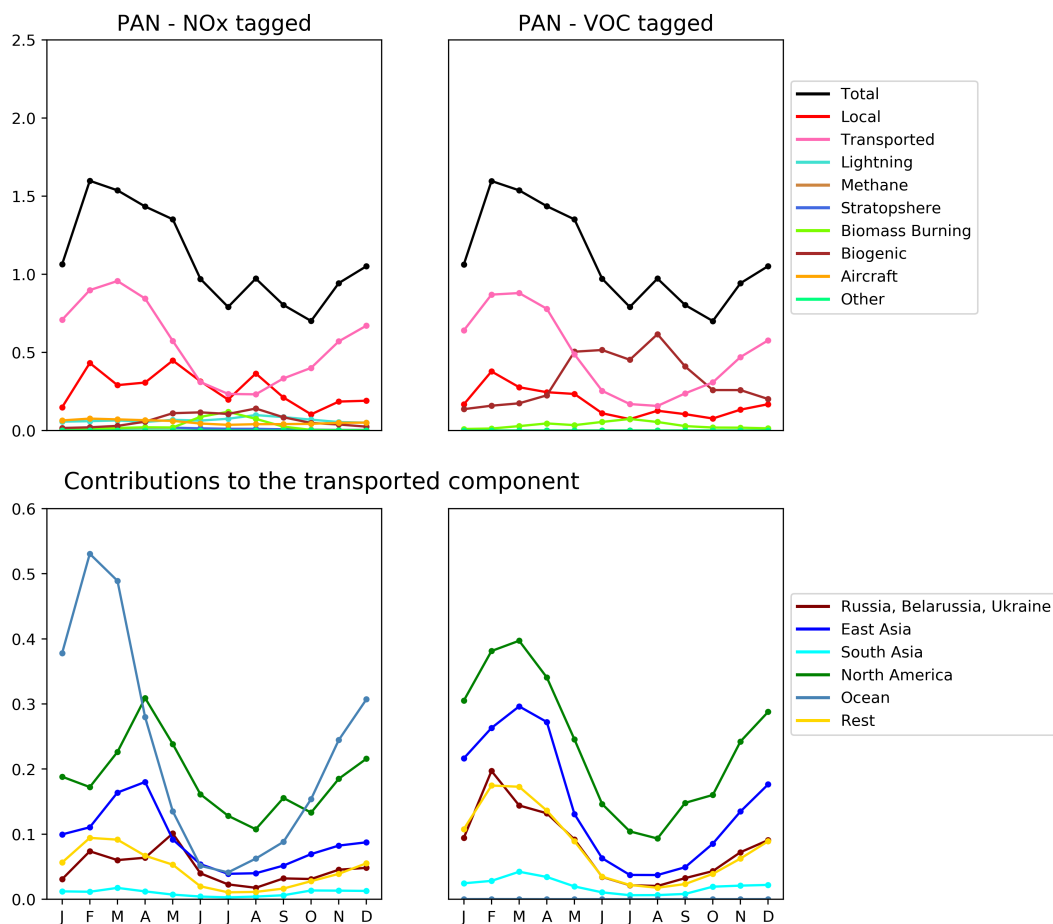


Figure 8. Seasonal cycle of column-integrated lower tropospheric PAN (10^{-15} molec cm^{-2}) in the HTAP Tier 2 receptor region “North West Europe”. The lower troposphere is defined here as all model levels between 800 and 500 hPa. NO_x -tagging is shown in the left panels, and reactive carbon tagging in the right panels. Top panels show total monthly mean PAN (black line) as well as the local anthropogenic component, long-range transported anthropogenic component, and natural components. Bottom panels show the individual Tier 1 source regions responsible for the long-range transported component of PAN.



Figure 9. Seasonal cycle of column-integrated lower tropospheric PAN (10^{-15} molec cm^{-2}) in the HTAP Tier 2 receptor region “North East China”. The lower troposphere is defined here as all model levels between 800 and 500 hPa. NO_x -tagging is shown in the left panels, and reactive carbon tagging in the right panels. Top panels show total monthly mean PAN (black line) as well as the local anthropogenic component, long-range transported anthropogenic component, and natural components. Bottom panels show the individual Tier 1 source regions responsible for the long-range transported component of PAN.

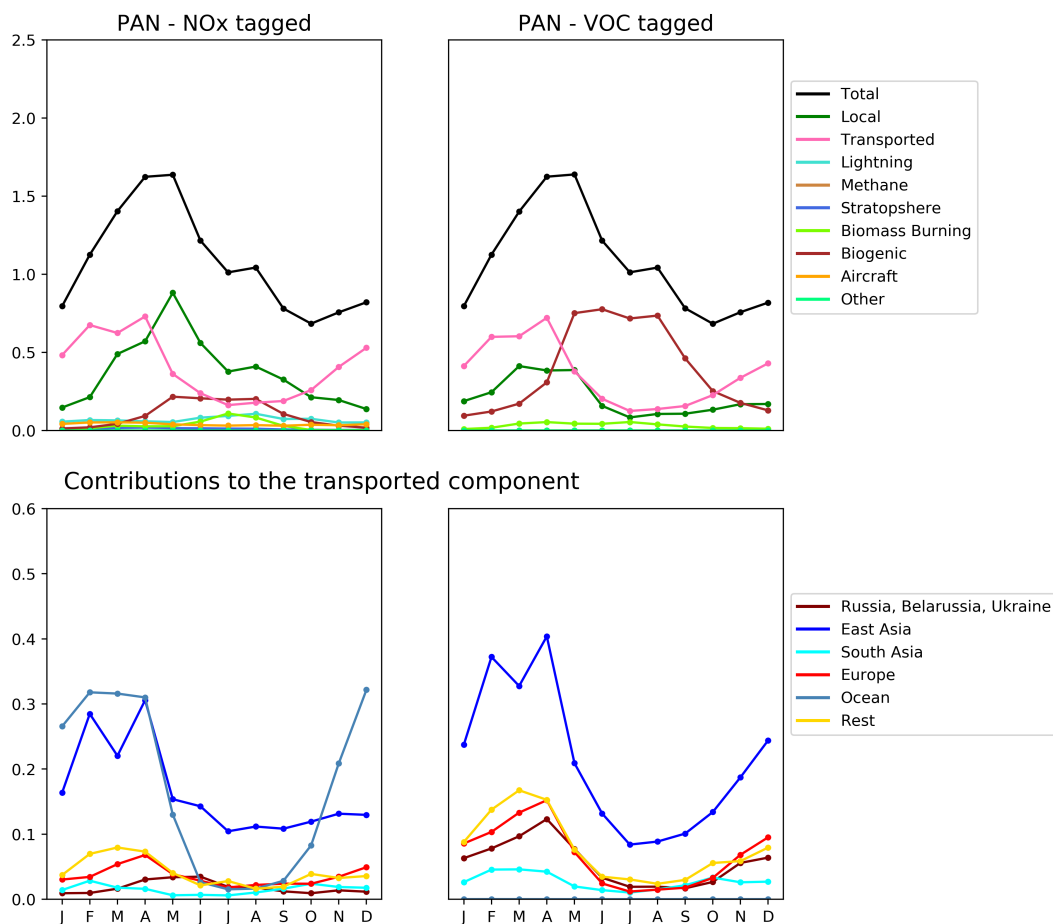


Figure 10. Seasonal cycle of column-integrated lower tropospheric PAN (10^{-15} molec cm^{-2}) in the HTAP Tier 2 receptor region “North West United States”. The lower troposphere is defined here as all model levels between 800 and 500 hPa. NO_x -tagging is shown in the left panels, and reactive carbon tagging in the right panels. Top panels show total monthly mean PAN (black line) as well as the local anthropogenic component, long-range transported anthropogenic component, and natural components. Bottom panels show the individual Tier 1 source regions responsible for the long-range transported component of PAN.

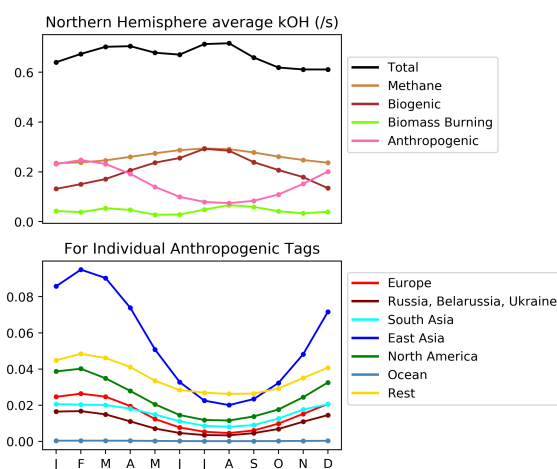


Figure 11. Seasonal cycle of northern hemispheric tropospheric column-integrated OH reactivity (s^{-1}) due to reactive carbon from the VOC-tagged run. The complete attribution is shown in the top panel, and the detailed attribution to anthropogenic emissions from HTAP Tier 1 source regions is shown in the bottom panel.



Table 1. List of tags used for attribution of tropospheric ozone in the NO_x- and VOC-tagged runs. Anthropogenic emissions of NO_x and reactive carbon are tagged based on their HTAP Tier 1 region. Other tags are as in Butler et al. (2018).

Tag name	NO _x -tagging	VOC-tagging
HTAP Tier 1 regions		
Oceans ¹	Explicit	Explicit
North America	Explicit	Explicit
Europe	Explicit	Explicit
South Asia	Explicit	Explicit
East Asia	Explicit	Explicit
Russia, Belarus, Ukraine	Explicit	Explicit
South East Asia	Explicit	RoW
Northern Africa	Explicit	RoW
Middle East	Explicit	RoW
Middle America	Explicit	RoW
Central Asia	Explicit	RoW
Pacific, Australia, New Zealand	RoW	RoW
Southern Africa	RoW	RoW
South America	RoW	RoW
Arctic	RoW	RoW
Antarctic	RoW	RoW
Other tags		
Stratosphere	Global ²	Global
Aircraft	Global	Global
Biogenic	Global	Global
Biomass burning	Global	Global
Lightning	Global	N/A
Methane	N/A	Global
Extra production	Global ³	Global ⁴

¹Both natural and anthropogenic emissions are included in “Oceans”.

²For NO_x tagging, the stratosphere tag is applied directly to ozone produced in the stratosphere (as for VOC tagging) and also to NO produced from dissociation of N₂O.

³For NO_x tagging, “extra production” of ozone is due to the self reaction of OH radicals and reactions between HO₂ and organic peroxy radicals.

⁴For VOC tagging, “extra production” of ozone is due to the self reaction of OH radicals and reaction of OH with H₂O₂.



Table 2. Attribution of ozone to tagged sources of NO_x . Also shown is the contribution of the stratosphere, and the contribution of minor chemical production pathways in the troposphere. Contributions of each tagged source are shown to both the 2010 annual average tropospheric burden and to the annual average Northern Hemisphere surface mixing ratio. Where applicable, the Ozone Production Efficiency (OPE) of NO_x emissions from each tagged source is also given.

NO_x Source	Emissions (Tg(N)/yr)	Ozone burden (Tg)	OPE (mol/mol)	NH surface (ppb)
Lightning	3.43	80.5	6.85	3.14
Stratosphere	–	75.5	–	3.17
Biogenic	5.04	26.0	1.50	2.57
Oceanic sources	4.28	19.9	1.35	5.33
East Asia	9.97	16.9	0.495	3.01
South East Asia	1.62	15.3	2.76	0.755
Aircraft	0.646	12.2	5.49	1.13
Biomass burning	5.03	12.1	0.704	1.45
South Asia	3.49	10.8	0.907	1.27
North America	4.79	10.4	0.632	2.88
Middle America	1.27	8.81	2.02	1.00
Europe	3.16	4.81	0.444	1.76
Middle East	1.82	4.11	0.659	1.02
RUS/BEL/UKR	1.37	2.15	0.457	0.852
North Africa	0.531	1.72	0.947	0.513
Central Asia	0.287	0.627	0.638	0.238
Rest of World	2.54	15.7	1.80	0.500
Extra production	–	1.47	–	0.132
Total trop. ozone	–	319	–	30.7



Table 3. Attribution of ozone to tagged sources of reactive carbon. Also shown is the contribution of the stratosphere, and the contribution of minor chemical production pathways in the troposphere. Contributions of each tagged source are shown to both the 2010 annual average tropospheric burden and to the annual average Northern Hemisphere surface mixing ratio. Where applicable, the Ozone Production Efficiency (OPE) of reactive carbon emissions from each tagged source is also given.

Reactive carbon source	Emissions		Ozone burden (Tg)	OPE (mol/mol)	NH surface (ppb)
	VOC (Tg(C)/yr)	CO (Tg(C)/yr)			
Methane	410	–	113	0.0689	12.4
Biogenic	668	42.2	76.8	0.0270	7.20
Stratosphere	–	–	66.8	–	2.91
Biomass burning	29.8	162	13.4	0.0176	1.25
East Asia	20.0	80.4	10.3	0.0257	1.96
South Asia	16.2	36.5	6.67	0.0316	0.715
North America	12.0	23.8	4.39	0.0307	1.18
Europe	6.12	11.6	2.04	0.0288	0.695
RUS/BEL/UKR	4.04	4.92	1.22	0.0341	0.433
Oceanic sources	11.0	0.587	0.0957	0.00206	0.0162
Rest of World	55.3	82.8	19.5	0.0352	1.43
Extra production	–	–	4.58	–	0.546
Total trop. ozone	–	–	319	–	30.7



Table 4. Change in the contribution of reactive carbon sources to tropospheric and Northern Hemisphere surface ozone in response to a 25% increase in the imposed surface mixing ratio of methane. Absolute changes and percentage changes are both shown.

Ozone source	Tropospheric Burden		NH Surface mixing ratio	
	Change in ozone burden (Tg)	Percentage change	Change in mixing ratio (ppb)	Percentage change
Methane	13.0	13.0	1.47	13.5
Biogenic	-1.88	-2.40	-0.168	-2.28
Stratosphere	-0.683	-1.01	-0.0226	-0.770
Rest of World	-0.379	-1.91	-0.0315	-2.15
Biomass burning	-0.243	-1.78	-0.0316	-2.47
East Asia	-0.238	-2.26	-0.0583	-2.90
South Asia	-0.131	-1.93	-0.0155	-2.13
Extra production	-0.0351	-0.761	-0.00890	-1.60
North America	-0.0975	-2.17	-0.0351	-2.88
Europe	-0.0479	-2.29	-0.0222	-3.09
RUS/BEL/UKR	-0.0286	-2.29	-0.0132	-2.96
Oceanic sources	-0.00287	-2.91	-0	-4.72
Aircraft	-0.00158	-2.59	-0	-3.81
Total trop. ozone	9.22	2.98	1.07	3.59



Table 5. Change in the contribution of NO_x sources to tropospheric and Northern Hemisphere surface ozone in response to a 25% increase in the imposed surface mixing ratio of methane. Absolute changes and percentage changes are both shown.

Ozone source	Tropospheric Burden		NH Surface mixing ratio	
	Change in ozone burden (Tg)	Percentage change	Change in mixing ratio (ppb)	Percentage change
Lightning	3.37	4.37	0.149	4.97
Stratosphere	-0.0598	-0.0791	0.00980	0.310
Biogenic	0.915	3.65	0.0861	3.47
Oceanic sources	1.04	5.53	0.287	5.70
East Asia	0.532	3.25	0.0884	3.02
Rest of World	0.557	3.68	0.0167	3.45
South East Asia	0.509	3.43	0.0214	2.92
Aircraft	0.558	4.81	0.0557	5.20
Biomass burning	0.277	2.34	0.0361	2.55
South Asia	0.395	3.78	0.0370	3.00
North America	0.340	3.38	0.0928	3.33
Middle America	0.313	3.68	0.0309	3.19
Europe	0.154	3.31	0.0559	3.29
Middle East	0.146	3.67	0.0389	3.96
RUS/BEL/UKR	0.0703	3.38	0.0269	3.26
North Africa	0.0736	4.46	0.0231	4.72
Extra production	0.00229	0.156	-0	-0.00590
Central Asia	0.0235	3.89	0.00936	4.09
Total trop. ozone	9.22	2.98	1.07	3.59